Manganese compounds with phthalate and terephthalate ligands: Synthesis, crystal structure, magnetic properties and catalase activity

Verónica Gómez [a,*], Montserrat Corbella [a,*], Franz A. Mautner [b], Olivier Roubeau [c], Simon J. Teat [d], Mercè Font-Bardia [e], Teresa Calvet [e]

[a] Departament de Química Inorgànica, Facultat de Química, Universitat de Barcelona, Martí i Franquès 1-11, 08028 Barcelona, Spain

[b] Institut für Physikalische and Theoretische Chemie, Technische Universität Graz, A-8010 Graz, Austria

[c] Instituto de Ciencia de Materiales de Aragón (ICMA), CSIC and Universidad de Zaragoza, Plaza San Francisco s/n, 50009 Zaragoza, Spain

[d] Advanced Light Source, Berkeley Laboratory, 1 Cyclotron Road, Berkeley, CA 94720, USA

[e] Cristal lografia, Mineralogia i Dipòsits Minerals, Universitat de Barcelona, Martí i Franquès s/n, 08028 Barcelona, Spain

* Corresponding authors. Fax: +34 934907725.

E-mail addresses: veronica.gomez@qi.ub.es (V. Gómez), montse.corbella@qi.ub. es (M. Corbella).

Abstract

The reactivity of carboxybenzoic acids substituted in ortho, meta and para positions (phthalic, isophthalic and terephthalic acids) has been explored. These acids have been used for the synthesis of dinuclear Mn^{III} and polynuclear Mn^{II} compounds, obtaining unexpected results. From all the reactions, one dinuclear Mn^{III} compound, $[\{Mn(H_2O)(phen)\}_2(\mu\text{-}2\text{-}COOHC_6H_4COO)_2(\mu\text{-}O)](ClO_4)_2$ (**1**), one mixed valence compound, $[\{Mn(phen)_2\}_2(\mu\text{-}O)_2](NO_3)_3$ (**2**), and four MnII compounds, $[\{Mn(H_2O)(phen)_2\}_2(\mu\text{-}4\text{-}COOC_6H_4\text{-}COO)](NO_3)_2$ (**3**), $[Mn_3(\mu\text{-}4\text{-}COOC_6H_4COO)_3(bpy)_2]n$ (**4**), $[\{Mn(phen)_2\}_2(\mu\text{-}2\text{-}COOHC_6H_4COO)_2](ClO_4)_2$ (**5**) and $[Mn(\mu\text{-}2\text{-}COOC_6H_4COO)(H_2O)_2(phen)]_n$ (**6**), (phen = 1,10-phenanthroline, bpy = 2,20-bipyridine) have been obtained and characterised by X-ray diffraction, showing different coordination modes for the carboxylate ligand: a bidentate bridge in a syn-syn, syn–anti or anti–anti mode, a bis-monodentate bridge and a bis-bidentate bridge. The six compounds show antiferromagnetic coupling, with magnetic interaction constants of -3.7 and -332.5 cm^{-1} for the dinuclear Mn^{III} (**1**) and $Mn^{III}Mn^{IV}$ (**2**) compounds and -0.04, -4.5, -1.5 and -0.55 cm^{-1} for Mn^{II} compounds **4–6**. Each Mn^{II} compound shows a different EPR spectrum at 4 K, which has been simulated including the ZFS parameters. The catalase activity of the compounds with phthalate and terephthalate ligands has been studied, the former being less active than the latter.

1. INTRODUCTION

Manganese-based coordination compounds are of great interest not only due to their magnetic properties [1] but also because of their importance in bioinorganic chemistry, as many manganese compounds are being synthesised to mimic several metalloproteins, such as the oxygen-evolving complex (OEC) of photosystem II [2] and catalase [3], an enzyme which catalyses the disproportionation of H_2O_2 into H_2O and O_2. This reaction is very important since hydrogen peroxide is one of the reactive oxygen species (ROS) associated with oxidative stress, which causes different diseases. High-resolution X-ray structures have been published for the Lactobacillus plantarum and Thermus thermophilus Mn-catalases [4], showing that their active site consists of two manganese ions with carboxylate ligands and the catalytic cycle involves the $Mn^{III}Mn^{III}$ and $Mn^{II}Mn^{II}$ states [5,6].

In our research group attention has been focussed on the synthesis and characterization of dinuclear Mn^{III} and polynuclear Mn^{II} compounds with carboxylate ligands in order to study their catalase activity [7–9]. Different benzoate ligands substituted with Cl, F and CH_3 groups have been used before. As a continuation, and with the aim of carrying on analyzing the effect of the substituent in the catalase activity, benzoate ligands with a second COOH group have been tested. There are very few Mn^{III} compounds reported in the literature, one dinuclear complex with a phthalate ligand [10], one chain with an isophthalate ligand [11] and two compounds with a terephthalate ligand (a dinuclear complex and a 1D system) [12]. Most of the compounds reported with these ligands are polynuclear Mn^{II} complexes [13–19], but only some of them have been magnetically characterised [13–17] and hardly any have had their EPR spectra recorded [15b].

Herein, we report the synthesis, crystal structure and magnetic properties of six compounds: $[\{Mn(H_2O)(phen)\}_2(\mu\text{-}2\text{-}COOHC_6H_4COO)_2(\mu\text{-}O)](ClO_4)_2$ (**1**), $[\{Mn(phen)_2\}_2(\mu\text{-}O)_2](NO_3)_3$ (**2**), $[\{Mn(H_2O)(phen)_2\}_2(\mu\text{-}4\text{-}COOC_6H_4COO)](NO_3)_2$ (**3**), $[Mn_3(\mu\text{-}4\text{-}COOC_6H_4COO)_3(bpy)_2]_n$ (**4**), $[\{Mn(phen)_2\}_2(\mu\text{-}2\text{-}COOHC_6H_4COO)_2]$ $(ClO_4)_2$ (**5**) and $[Mn(l\text{-}2\text{-}COOHC_6H_4COO)(H_2O)_2(phen)]_n$ (**6**). The EPR spectra of the Mn^{II} compounds have been recorded and simulated. The catalase activity of the Mn^{III} and Mn^{II}

79   compounds has been studied, as well as that of an analogous dinuclear Mn^{III} compound

80   reported in the literature, [{Mn(bpy)(H$_2$O)}$_2$(l-2-COOHC$_6$H$_4$COO)$_2$ (l-O)](NO$_3$)$_2$ (**A**)

81   [10], whose structure reveals two dinuclear entities, one with two coordinated water

82   molecules and another one with one nitrate ligand.

83

84

85

86

87

2. EXPERIMENTAL

2.1. Synthesis

All manipulations were carried out at room temperature under aerobic conditions. Reagents and solvents were obtained from commercial sources and used without further purification. NBu_4MnO_4 was prepared as described in the literature [20]. [Mn(4-$COOC_6H_4COO)(H_2O)_2]_n$ was synthesized by the reaction of $MnCO_3$ and terephthalic acid in boiling water. After several hours, the solution was filtered and concentrated under reduced pressure, giving a pale pink precipitate of the desired product [21]. Yields were calculated for a stoichiometric reaction. *Caution!* Perchlorate salts of compounds containing organic ligands are potentially explosive. Only small quantities of these compounds should be prepared and handled behind suitable protective shields.

*2.1.1. Preparation of [{Mn(H$_2$O)(phen)}$_2$(μ -2-COOHC$_6$H$_4$COO)$_2$ (μ-O)](ClO$_4$)$_2$ (**1**)*

Phthalic acid (0.27 g, 1.60 mmol) in CH_3CN was added to a solution of $Mn(ClO_4)_2 \cdot 6H_2O$ (0.46 g, 1.28 mmol) in the same solvent. Then, NBu_4MnO_4 (0.11 g, 0.32 mmol) dissolved in CH_3CN was added to the above-mentioned solution, which immediately turned dark brown. Finally, a CH_3CN solution of 1,10-phenanthroline (phen·H_2O) (0.35 g, 1.60 mmol) was added. The resulting solution (total volume ~35 mL) was stirred for 15 min and the solution was left undisturbed in a refrigerator. Slow evaporation of the mother liquor led to the precipitation of a dark solid. Yield 19% (0.17 g). Dark crystals suitable for X-ray diffraction were obtained by slow evaporation of the mother liquor. Anal. Calc. for $C_{40}H_{30}Cl_2Mn_2N_4O_{19} \cdot 0.6CH_3CN \cdot 2H_2O$ (1112.12): C, 44.49; H, 3.24; N, 5.79; Cl, 6.38. Found: C, 44.1; H, 3.1; N, 5.6; Cl, 6.6%. Selected IR data (KBr pellet, cm^{-1}): 3412(vs), 1709(vs), 1606(s), 1587(s), 1568(s), 1519(m), 1428(m), 1382(vs), 1109(vs), 1081(vs), 875(w), 850(m), 739(m), 720(s), 637(m), 625(m).

2.1.2. Preparation of [{Mn(bpy)(H2O)}2(μ -2-COOHC6H4COO)2(μ - O)](NO3)2 (A)

The same procedure for the preparation of compound **1** was followed, using Mn(NO$_3$)$_2$·4H$_2$O (0.32 g, 1.28 mmol) and 2,2'-bipyridine (0.25 g, 1.60 mmol). The resulting solution (total volume ~100 mL in this case) was stirred for 15 min and a small quantity of brown residue was filtered. Slow evaporation of the mother liquor led to the precipitation of the desired dark product. Yield 27% (0.16 g). Anal. Calc. for C$_{72}$H$_{58}$Mn$_4$N$_{12}$O$_{33}$ (1839.04): C, 47.02; H, 3.18; N, 9.14. Found: C, 47.5; H, 3.0; N, 9.5%. Selected IR data (KBr pellet, cm^{-1}): 3408(s), 1736(vs), 1610(s), 1589(s), 1496(w), 1470(m), 1447(s), 1384(vs), 1307(s), 1075(m), 1033(m), 772(s), 728(s), 662(w).

2.1.3. Preparation of [{Mn(phen)2}2(μ -O)2](NO3)3 (2)

Phthalic acid (0.27 g, 1.60 mmol) in CH$_3$CN was added to a solution of Mn(NO$_3$)$_2$·4H$_2$O (0.32 g, 1.28 mmol) in the same solvent. Then, NBu$_4$MnO$_4$ (0.11 g, 0.32 mmol) dissolved in CH$_3$CN was added to the above-mentioned solution, which immediately turned dark brown. Finally, a CH$_3$CN solution of phen·H$_2$O (0.32 g, 1.60 mmol) was added. The resulting solution (total volume ~75 mL) was stirred for 15 min and filtered to remove a dark brown solid. The solution was left undisturbed in a refrigerator. Slow evaporation of the mother liquor led to the formation of dark crystals suitable for X-ray diffraction. Yield: 8% (0.04 g). Anal. Calc. for C$_{48}$H$_{32}$Mn$_2$N$_{11}$O$_{11}$·2-COOHC$_6$H$_4$COOH·3H$_2$O (1268.88): C, 53.01; H, 3.50; N, 12.14. Found: C, 53.2; H, 3.4; N, 12.2%. Selected IR data (KBr pellet, cm^{-1}): 3424(s), 1729(w), 1715(w), 1634(w), 1579(w), 1518(m), 1425(m), 1384(vs), 849(m), 719(m), 689(m), 657(w), 638(w), 595(w).

2.1.4. Preparation of [{Mn(H2O)(phen)2}2(μ -4-COOC6H4COO)](NO3)2 (3)

[Mn(4-COOC$_6$H$_4$COO)(H$_2$O)2]n (0.03 g, 0.12 mmol) and HNO$_3$ (125 μL 1.4 Min ethanol) were mixed in ethanol, leading to a white suspension due to the low solubility of the manganese carboxylate. Then phen·H$_2$O (0.05 g, 0.24 mmol), dissolved in the same

solvent, was added to the above-mentioned suspension (total volume 20 mL) and the resulting suspension was stirred for 15 min and filtered to remove the non-reacted manganese carboxylate. Crystals suitable for X-ray diffraction were obtained by slow evaporation of the mother liquor in a refrigerator. Yield: 4% (0.003 g). Anal. Calc. for $C_{56}H_{40}Mn_2N_{10}O_{12}\cdot0.5CH_3CH_2OH$ (1177.89): C, 58.12; H, 3.68; N, 11.89. Found: C, 58.1; H, 3.4; N, 11.7%. Selected IR data (KBr pellet, cm^{-1}): 3423(m), 1622(w), 1561(m), 1516(m), 1424(s), 1384(vs), 1341(m), 1101(m), 866(w), 846(m), 727(s), 638(m).

2.1.5. Preparation of [Mn3(μ -4-COOC6H4COO)3(bpy)2]n (4)

$Mn(NO_3)_2\cdot4H_2O$ (0.05 g, 0.20 mmol) and 2,20-bipyridine (bpy) (0.02 g, 0.13 mmol) were dissolved in 10 mL of ethanol and this solution was layered with terephthalic acid (0.03 g, 0.20 mmol) dissolved in dimethylformamide (DMF). Crystals suitable for X-ray diffraction were obtained by liquid–liquid diffusion. Yield: 34% (0.03 g). Anal. Calc. for $C_{44}H_{28}Mn_3N_4O_{12}\cdot DMF\cdot0.5H_2O$ (1051.62): C, 53.68; H, 3.45; N, 6.66. Found: C, 53.6; H, 3.4; N, 6.5%. Selected IR data (KBr pellet, cm^{-1}): 3423(m), 1677(m), 1603(s), 1500(w), 1474(w), 1439(m), 1385(s), 1016(w), 747(m), 525(m).

2.1.6. Preparation of [{Mn(phen)2}2(μ -2-COOHC6H4COO)2](ClO4)2 (5)

KOH (0.02 g, 0.50 mmol) in 3 mL of water was added to a solution of phthalic acid (0.08 g, 0.50 mmol) in acetone. Then $Mn(ClO_4)_2\cdot6H_2O$ (0.10 g, 0.50 mmol) and $phen\cdot H_2O$ (0.20 g, 1.0 mmol) dissolved in acetone were added and the resulting solution (total volume 25 mL) was stirred for 15 min. Crystals suitable for X-ray diffraction were obtained by liquid–liquid diffusion, layering the acetone solution with $CHCl_3$. Yield: 11% (0.025 g). Anal. Calc. for $C_{64}H_{42}Cl_2Mn_2N_8O_{16}\cdot3H_2O$ (1413.89): C, 54.36; H, 3.42; N, 7.93; Cl, 5.01. Found: C, 54.1; H, 3.4; N, 7.5; Cl, 5.4%. Selected IR data (KBr pellet, cm^{-1}): 3418(w), 1682(m), 1604(s), 1591(s), 1574(s), 1517(s), 1425(s), 1406(s), 1103(s), 865(w), 847(m), 756(m), 729(s), 623(m).

2.1.7. Preparation of [Mn(μ-2-COOC6H4COO)(H2O)2(phen)]n (6)

171   Mn(CH$_3$COO)$_2$·4H$_2$O (0.12 g, 0.50 mmol) and phthalic acid (0.08 g, 0.50 mmol),

172   both dissolved in 20 mL of water, were added to an ethanolic solution (20 mL) of phen·H$_2$O

173   (0.10 g, 0.50 mmol) and stirred for 15 min. Crystals suitable for X-ray diffraction were

174   obtained by slow evaporation of the mother liquor at room temperature. Yield: 53% (0.12

175   g). Anal. Calc. for C$_{20}$H$_{16}$MnN$_2$O$_6$·H$_2$O (453.30): C, 52.99; H, 4.00; N, 6.18. Found: C,

176   52.5; H, 3.9; N, 6.1%. Selected IR data (KBr pellet, cm^{-1}): 3447(m), 3275(m), 1547(s),

177   1516(m), 1430(m), 1410(m), 1394(m), 861(w), 850(m), 757(m), 727(m).

178

179   *2.2. Physical measurements*

180   Analyses of C, H, N and Cl were carried out by the Servei de Microanàlisi of the

181   Consell Superior d'Investigacions Científiques (CSIC). Infrared spectra were recorded on

182   KBr pellets in the range 4000–400 cm^{-1} with a Thermo Nicolet Avatar 330 FT-IR

183   spectrometer. Magnetic susceptibility measurements (2–300 K) and magnetization

184   measurements at 2 K, (0–50000 G), were carried out in a Quantum Design MPMP SQUID

185   Magnetometer at the Unitat de Mesures Magnètiques (Universitat de Barcelona). Two

186   different magnetic fields were used for the susceptibility measurements, 300 G (2–5 K) and

187   3000 G (2–300 K), with superimposable graphs. Pascal's constants were used to estimate

188   the diamagnetic corrections for the compounds. The fits were performed by minimising the

189   function R = $R[(\chi_M T)_{exp} - (\chi_M T)_{calc}]^2 / R[(\chi_M T)_{exp}]^2$. Solid-state EPR spectra were

190   recorded at the X-band (9.4 GHz) frequency using a Bruker ESP-300E spectrometer, from

191   room temperature to 4 K at the Unitat de Mesures Magnètiques (Universitat de Barcelona).

192   The computational package easyspin [22] was used to simulate the EPR spectra of the

193   compounds.

194

195   *2.3. Crystal structure determination and refinement*

196   X-ray diffraction measurements and resolution of compounds **1** and **3** were carried

197   out at station 11.3.1 of the Advanced Light Source at Lawrence Berkeley National

198   Laboratory. All measurements were made at 100 K on a Bruker APEX II CCD

diffractometer with a silicon 111 monochromator ($\lambda = 0.7749$ Å). Compound **2** was elucidated at the European Synchrotron Radiation Facility BM16 (Grenoble). All measurements were made at 150 K on a Single-axis HUBER diffractometer with a silicon 111 monochromator ($\lambda = 0.75150$ Å). X-ray diffraction measurements and resolution of compound **5** were carried out at the Unitat de Difracció de Raigs X (Serveis Cientificotècnics, Universitat de Barcelona). All measurements were made at 105 K on a MAR345 diffractometer with an image plate detector and graphite monochromated Mo Kα radiation ($\lambda = 0.7107$ Å). Compounds **6** and **4** were elucidatedat the Institut für Physikalische and Theoretische Chemie (Technische Universität Graz). All measurements were made at 100 K on a Bruker P4 diffractometer with graphite monochromated Mo Kα radiation ($\lambda = 0.7107$ Å). Compound **1** was solved and refined with the SHELX-TL suite [23,24], compound **3** was solved with the SIR97 program [25] and refined with the SHELX-TL suite, and compounds **2**, **4**, **5** and **6** were solved with the SHELXS97 program [23,24] and refined with the SHELX97 program. Crystal data collection and refinement parameters for all compounds (**1**–**6**) are given in Table 1.

2.4. Catalase activity

The study of the catalase activity (disproportionation reaction of H_2O_2 into H_2O and O_2) was carried out at 25 °C by volumetric determination of the oxygen evolved with a gas-measuring burette (with a precision of 0.1 mL). Three different initial quantities of H_2O_2 30% (0.50, 0.60 and 0.70 mL) were added to closed vessels containing 5.0 mL of CH_3CN solutions 0.8 mMof the dinuclear Mn^{III} compounds **1** and **A** and Mn^{II} compounds **3**–**6**. Blank experiments carried out without the catalyst showed negligible disproportionation of H_2O_2.

3. RESULTS AND DISCUSSION

3.1. Synthesis

The majority of the substituted benzoic acids used in our group (RC_6H_4COOH, R = n-Cl, n-F, n-CH_3) for the synthesis of dinuclear Mn^{III} compounds lead satisfactorily to complexes with the general formula $[\{Mn(L)(NN)\}_2(\mu\text{-}RC_6H_4COO)_2(\mu\text{-}O)]X_2$ [8,9,26–30]. This synthesis consists of a comproportionation reaction between a Mn^{II} salt and NBu_4MnO_4 in the presence of the acid and a bidentate ligand, using acetonitrile or ethanol as solvent. However, analogous reactions with benzoic acids with a second COOH group, bpy/phen and nitrate/perchlorate only lead to the formation of two dinuclear Mn^{III} compounds, both with the substituent in the ortho position (phthalic acid): $[\{Mn(H_2O)(phen)\}_2(\mu\text{-}2\text{-}COOHC_6H_4COO)_2(\mu\text{-}O)](ClO_4)_2$ (1) and $[\{Mn(bpy)(H_2O)\}(\mu\text{-}2\text{-}COOHC_6H_4COO)_2(\mu\text{-}O)\{Mn(bpy)(H_2O/NO_3)\}](NO_3)_{1/2}$ (A). This latter compound has been reported in the literature, but the synthetic procedure is different since it was obtained as a byproduct by the oxidation of a Mn^{II} solution [10]. The rest of the synthesis gave rise to the formation of known dinuclear $Mn^{III}Mn^{IV}$ compounds with the general formula $[\{Mn(NN)_2\}_2(\mu\text{-}O)_2]X_3$ and the precipitation of the acid (Fig.1). For the reaction of phthalic acid, $Mn(NO_3)_2$ and phen, the compound $[\{Mn(phen)_2\}_2(\mu\text{-}O)_2](NO_3)_3$ (2) with phthalic acid acting as molecule of crystallization was obtained. Although several reaction conditions and reactants were used to try and achieve dinuclear Mn^{III} compounds, these were unsuccessful. However, two Mn^{II} compounds were obtained with terephthalic acid. The dinuclear compound $[\{Mn(H_2O)(phen)_2\}_2(\mu\text{-}4\text{-}COOC_6H_4COO)](NO_3)_2$ (3) was formed using $[Mn(4\text{-}COOC_6H_4\text{-}COO)(H_2O)_2]n$ as a starting material and HNO_3 in ethanol. It can also be obtained without NBu_4MnO_4, but the use of HNO_3 is necessary; another nitrate source gave rise to the formation of neutral compounds. However in both cases, the yield is very low as manganese(II) terephthalate is quite insoluble in ethanol. Other attempts to synthesize compound 3 using manganese(II) acetate or nitrate and terephthalic acid lead to neutral compounds. The second compound is the 2D system $[Mn_3(\mu\text{-}4\text{-}$

252 $COOC_6H_4COO)_3(bpy)_2]_n$ (4), obtained in a mixed DMF-ethanol solution using $Mn(NO_3)_2$.

253 It is also obtained without NBu_4MnNO_4, with a better yield. Although the

254 comproportionation reaction initially takes place, the Mn^{III} ions formed are reduced to Mn^{II}

255 by ethanol, probably due to a poor stabilization of the oxidized state.

256   Once again, the use of Mn^{II} sources and phthalic/isophthalic/terephthalic acid to

257 obtain polynuclear Mn^{II} compounds contrasts with the synthetic procedure used until now

258 by our research group (Fig. 1). We have reported several Mn^{II} compounds with

259 chlorobenzoate and chloroacetate ligands [31] and the use of $[Mn(RCOO)_2]$ as a starting

260 material was necessary, otherwise compounds with no carboxylate ligands were obtained.

261 However in this case, analogous procedures using $[Mn(n\text{-}COOC_6H_4COO)_2]_n$ were

262 unsuccessful, maybe due to the polymeric character of these compounds. Only compound 3

263 was obtained using manganese terephthalate, the use of HNO_3 being necessary. The

264 dinuclear Mn^{II} compound $[\{Mn(phen)_2\}_2(\mu\text{-}2\text{-}COOHC_6H_4COO)_2](ClO_4)_2$ (5) was

265 obtained by the reaction of $Mn(ClO_4)_2$, phthalic acid, phen and KOH in acetone. The use of

266 $Mn(NO_3)_2$ gave rise to the formation of the neutral Mn^{II} one-dimensional system $[Mn(\mu\text{-}$

267 $2\text{-}COOC_6H_4COO)(H_2O)_2(phen)]_n$ (**6**), instead of obtaining an ionic compound, despite the

268 presence of nitrate anions. In both cases, the use of KOH is crucial to obtain these products,

269 otherwise compounds without phthalate ligands are obtained: $[\{Mn(phen)_2\}_2(\mu\text{-}$

270 $O)_2](ClO_4)_3$ (oxidation of Mn^{II} in the air) and $[Mn(phen)_3](NO_3)_2$, respectively.

271 Nevertheless, compound **6** can be obtained more efficiently using $Mn(CH_3COO)_2$ as a Mn^{II}

272 source, and it is not necessary to add KOH in this case.

273   The compounds reported here show different coordination modes depending on the

274 position of the second carboxylate group, as determined from the single-crystal structures

275 (see next section). In compounds with the phthalate ligand (*ortho*-substituted), only one

276 carboxylate group is involved in the coordination, leading to $\mu_{1,3}$ bridges with *syn-syn* (**1**),

277 *syn-anti* (**5**) or *anti-anti* (**6**) conformations. On the contrary, in compounds with terephthalate

278   ligands (para-substituted), both carboxylate groups are coordinated to the manganese ions,

279   with a bis-monodentate coordination mode (**3**) or using the four oxygen atoms (**4**).

280   The IR spectra of these compounds show two strong bands at ~1580 and ~1390 cm⁻

281   ¹ due to the asymmetric and symmetric vibrations of the COO groups. The values of $\Delta =$

282    $v_a(COO)$ - $v_s(COO)$, being ~200 cm⁻¹ for compounds **1, 4, 5** and **6**, are indicative of

283   carboxylate ligands coordinated in a bidentate bridging mode ($\mu_{1,3}$) [32], while higher

284   values are expected for compound **3**, with a monodentate coordination, although hydrogen

285   bonds may decrease this Δ value. Moreover, the presence of COOH groups in compounds

286   **1, 2** and **5** leads to another band at ~1700 cm⁻¹. On the other hand, broad bands at ~1100

287   cm⁻¹ and a moderate intensity band at 623 cm⁻¹ in the spectrum of compounds **1** and **5** are

288   assigned to the perchlorate anions, and a very intense band at 1384 cm⁻¹ in the spectrum of

289   compound **3** corresponds to nitrate anions. The phen ligand shows characteristic bands at

290   ~1516, 1428, 863, 848 and 727 cm⁻¹ and the bpy ligand at ~1500, 1474 and 1439 cm⁻¹.

291

292   *3.2. Description of the structures*

293   *3.2.1. [{Mn(H₂O)(phen)}₂ (μ-2-COOHC₆H₄COO)₂ (μ-O)](ClO₄)₂ · 0.6CH₃CN·2H₂O*

294   (**1**·*0.6CH₃CN·2H₂O*)

295   The crystal structure of compound **1**·0.6CH₃CN·2H₂O shows a dinuclear cation, two

296   perchlorate anions and acetonitrile and water molecules. The structure of the cationic

297   complex is shown in Fig. 2 and selected bond lengths and angles are given in Table 2. The

298   two Mn(III) ions are bridged by one oxo and two $\mu_{1,3}$-phthalato ligands, in a syn-syn mode,

299   with a Mn···Mn distance of 3.151 Å and a Mn – O - Mn angle of 123.2°. The Mn - O bond

300   lengths of the oxo bridge are ~ 1.79 Å and those of the carboxylate bridges are ~ 1.96 and

301   2.18 Å, the longer ones corresponding to the oxygen atoms placed trans to the molecules of

302   water. Each manganese ion is chelated by a phen ligand, with Mn - N distances of ~ 2.07 Å,

303   and the hexacoordination is completed by a molecule of water, the Mn – O distance being

304 ~2.23 Å. The structural parameters found for this compound agree with those reported for

305 analogous compounds with the same $[Mn_2(\mu\text{-}O)(\mu\text{-}RCOO)_2]^{2+}$ core [7–10,26–29,33,34].

306   Both manganese ions display an elongated coordination environment towards the

307 monodentate ligand direction due to the Jahn–Teller effect. The relative disposition of the

308 manganese coordination octahedra is almost perpendicular, with an O10–Mn1–Mn2–O11

309 torsion angle of 91.3°. The torsion angles between the carboxylate group coordinated to the

310 Mn ions and the phenyl ring are very different in each phthalate ligand. This angle, measured

311 as O – C – C - C, the oxygen atom being the one placed trans to the monodentate ligand, is

312 41.62° for Mn1 and 4.3° for Mn2. This big difference could be due to different inter and/or

313 intramolecular interactions within the crystal. The other two carboxylic groups are more

314 twisted, one being practically perpendicular to the phenyl ring.

315   The dinuclear complexes interact through hydrogen bonds between the coordinated

316 water molecules, perchlorate anions and free COOH groups (Fig.3). The water molecules

317 coordinated to the Mn1 ions (O10) interact through two water molecules and one perchlorate

318 anion, which is also hydrogen-bonded to the water molecule coordinated to the Mn2 ion

319 (O11). This water molecule also interacts with another perchlorate anion, which interacts

320 with the OH group of a phthalate ligand of a second dinuclear entity. The O· · ·O distances

321 are in the range 2.700–3.166 Å. Moreover, an acetonitrile molecule interacts with a water

322 molecule with a O2W· · ·N1S distance of 2.743 Å.

323

324 *3.2.2. [{Mn(phen)$_2$}$_2$(μ-O)$_2$](NO$_3$)$_3$·2-COOHC$_6$H$_4$COOH·2CH$_3$CN (2·2-*

325 *COOHC$_6$H$_4$COOH·2CH$_3$CN)*

326   The crystal structure of compound **2**·2-COOHC$_6$H$_4$COOH· 2CH$_3$CN consists of a

327 dinuclear cation, three nitrate anions, a molecule of phthalic acid and two molecules of

328 acetonitrile. As this kind of compound is quite well known, the cationic structure and

329 selected bond lengths and angles are shown in Fig. S1 and Table S1. Both manganese ions

330 are bridged by two oxo groups, leading to an almost planar Mn$_2$O$_2$ core (with an angle

331 between the O – Mn - O planes of ~ 0.1°), with a Mn· · ·Mn distance of 2.703 Å. The

332 hexacoordination is completed by two phen ligands. The manganese ions are in different

333 oxidation states, giving a mixed-valence Mn^{III}Mn^{IV} complex. In this case is possible to

distinguish both ions by comparing the Mn - ligand distances due to the Jahn–Teller effect characteristic of Mn[III] ions. According to this, the Mn1 ion shows a coordination environment elongated in the direction of the N1 and N4 atoms, being the Mn[III] ion, and thus Mn2 is the Mn[IV] ion. All structural parameters agree with those for analogous compounds [35,36].

The dinuclear entities are linked through π - π interactions between phen ligands of neighboring molecules, with a distance between the centroids of 3.544 Å (cycles involving N3 atoms). There are also several $C – H \cdots O$ and $C – H \cdots N$ interactions with nitrate anions and acetonitrile molecules. Moreover, the presence of phthalic acid leads to the formation of hydrogen bonds with nitrate anions, the $O \cdots O$ distances being in the range 2.656–3.188 Å.

3.2.3. $[\{Mn(H_2O)(phen)_2\}_2(\mu\text{-}4\text{-}COOC_6H_4COO)](NO_3)_2 \cdot 2CH_3CH_2OH$ ($3 \cdot 2CH_3CH_2OH$)

The crystal structure of compound $3 \cdot 2CH_3CH_2OH$ consists of a cationic complex, two nitrate anions and two molecules of ethanol. The cationic complex is depicted in Fig. 4 and selected bond lengths and angles are listed in Table 3. Each manganese ion coordinates to two phen ligands, a molecule of water and one monodentate terephthalate ligand, which acts as a bis-monodentate bridge, leading to a $Mn \cdots Mn$ distance of 11.517 Å. The Mn - N distances are ~2.27 Å and both Mn - O distances are 2.119 Å. The carboxylate groups and the phenyl ring of the terephthalate ligand are almost coplanar, with a torsion angle of only ~2°. This ligand is placed in such a way that the non-coordinated oxygen atoms interact through hydrogen bonds with the molecules of water, with a $O2 \cdots O3$ distance of 2.667 Å, stabilizing the molecular conformation.

The coordinated molecules of water also interact through hydrogen bonds with nitrate anions, with an $O3 \cdots O5$ distance of 2.703 Å. (Fig. S2). The nitrate anions also form another hydrogen bond with ethanol molecules, the $O6 \cdots O1S$ distance being 2.802 Å.

An analogous compound with a perchlorate anion instead of the nitrate anion is found in the literature [14]. The main structural difference lies in the Mn - O distances; compound **3** shows two almost identical distances, while in the other compound these distances are different, the distance corresponding to the oxygen atom of the molecule of water being

363   larger (2.142 Å). There are two more dinuclear Mn^{II} compounds bridged by just one

364   terephthalate bridge reported in the literature [15]. Among the four complexes, compound **3**

365   shows the largest Mn· · ·Mn distance (11.210–11.456 Å).

366

367   *3.2.4. [Mn$_3$(μ-4-COOC$_6$H$_4$COO)$_3$(bpy)$_2$]$_n$·0.75DMF·0.25H$_2$O(4·0.75DMF·0.25H$_2$O)*

368   The crystal structure of compound **4**·0.75DMF·0.25H$_2$O consists of a 2D

369   coordination framework and disordered lattice molecules of DMF and water. This two-

370   dimensional system is formed by trinuclear units connected by terephthalate ligands (Fig.

371   5). Selected bond lengths and angles are gathered in Table 4. Each unit consists of a linear

372   array of three Mn^{II} ions, where the central manganese ion is located on a crystallographic

373   inversion centre. The central Mn2 ion coordinates to six oxygen atoms of six terephthalate

374   ligands, with Mn - O distances in the range 2.113–2.206 Å, and it is linked to the two terminal

375   manganese ions through three carboxylate bridges, with a Mn1· · ·Mn2 distance of 3.526 Å.

376   Two of these bridges are in a $μ_{1,3}$ syn–syn coordination mode, while the third carboxylate

377   bridge shows a $μ_{1,1}$ coordination mode, the Mn1 - O1 - Mn2 angle being 106.51°. The non-

378   coordinated oxygen atom is weakly bonded to the terminal manganese ion, with a Mn1 - O2

379   distance of 2.389 Å, and these terminal manganese ions complete their hexacoordination

380   with a bpy ligand (Mn - N distances ~2.26 Å).

381   The trinuclear entity shows a structure analogous to several trinuclear compounds

382   with a [Mn$_3$($μ_{1,3}$-RCOO)$_4$($μ_{1,1}$-RCOO)$_2$] core, the structural parameters being comparable

383   to those reported in the literature [37]. The existence of another carboxylate group in the

384   para position leads to the connection of the trinuclear entities to generate a 2D system, as

385   shown in Fig. 5.

386   This topology is also found in other compounds with terephthalate ligands [16a–c].

387   One of them corresponds to this same compound, but with different structural parameters

388   [16a]. The main difference corresponds to the carboxylate bridge with the $μ_{1,1}$ coordination

389   mode. Compound **4** shows a larger Mn – O – Mn angle (106.51° in contrast to 105.74°) and

390   a slightly shorter Mn – O distance (2.195° in contrast to 2.206 Å). Moreover, the distance

391 between the terminal manganese ion and the non-bridging ligand is also shorter (2.389° in
392 contrast to 2.417 Å).

393

394 *3.2.5. [{Mn(phen)$_2$}$_2$(μ-2-COOHC$_6$H$_4$COO)$_2$](ClO$_4$)$_2$·3CHCl$_3$·4H$_2$O(5·3CHCl$_3$ - 4H$_2$O)*

395   The crystal structure of compound **5**·3CHCl$_3$·4H$_2$O shows a dinuclear cation, two
396 perchlorate anions, three chloroform molecules and four molecules of water (one of them
397 with 50% disorder). The cationic structure is shown in Fig. 6 and selected bond lengths and
398 angles are listed in Table 5. The Mn^{II} ions are bridged by two μ$_{1,3}$-carboxylate ligands in a
399 syn–anti mode, with a Mn· · ·Mn distance of 4.790 Å. Both phthalate ligands act as mono-
400 bidentate ligands, using just one carboxylate group to bridge two manganese ions, with the
401 other carboxylate group, being protonated, remaining free. No COO groups are coplanar to
402 the phenyl ring, the torsion angles being ~62.7° and 27.9° for the coordinated and free ones.
403 The hexacoordination of each manganese ion is completed by two phen ligands, leading to
404 a distorted octahedral environment around the Mn^{II} ions, with Mn - O distances much shorter
405 than the Mn - N distances (~2.14 and 2.27 Å, respectively). All distances agree with those
406 reported for analogous compounds [14,37].

407   The dinuclear complexes interact through hydrogen bonds between the free COOH
408 groups, leading to 1D chains (Fig. S3). Two different interactions can be observed, which
409 alternate along the chain. The water molecule O4W bridges two dinuclear units through two
410 hydrogen bonds with the COOH groups, the O8· · ·O4W and O4W· · ·O7a distances being
411 2.547 and 2.647 Å, respectively (a: -x, 1 - y, -z), and it also interacts with a perchlorate anion,
412 with an O4W· · ·O13 distance of 2.790 Å. The second interaction takes place through two
413 COOH groups in a direct way, with an O3· · ·O4a distance of 2.626 Å.

414   There are three compounds with the same dinuclear entity reported in the literature,
415 although with different anion/lattice solvent [15]. However in those cases, the two
416 manganese ions are equivalent. Moreover, compound **5** shows longer Mn - O distances and
417 a Mn· · ·Mn distance much shorter than an analogous compound which also has perchlorate
418 anions (4.790 and 4.836 Å, respectively) [15a].

419

420

3.2.6. [Mn(μ-2-COOC_6H_4COO)(H_2O)_2(phen)]_n·H_2O (6·H_2O)

The crystal structure of compound **6**·H_2O consists of a neutral 1D system and molecules of water. A fragment of this chain is shown in Fig. 7 and selected bond lengths and angles are gathered in Table 6.

This compound consist of an infinite chain of Mn^{II} ions placed linearly and bridged by just one phthalate ligand in a $\mu_{1,3}$ anti–anti coordination mode, with a Mn· · ·Mn distance of 6.420 Å. The manganese ions show two phthalate ligands trans to each other and they complete their hexacoordination with a phen ligand and two molecules of water. The Mn - N distances are ~2.28 Å and the Mn - O distances are ~2.19 and 2.14 Å, corresponding to the oxygen atoms of phthalate ligands and water, respectively. It is interesting to note that, differing from compounds **1** and **5**, the phthalate ligands in compound **6** are completely deprotonated, although just one carboxylate group participates in the coordination. The COO groups are twisted with respect to the phenyl rings, with a torsion angle of ~54.4°.

Along the chain, the ligands are placed in such a way that all the aromatic rings of the phthalate and phen ligands are located on one side and the non-coordinated carboxylate groups and the molecules of water on the other side (Fig. S4). These ligands form intramolecular hydrogen bonds with O6· · ·O3, O6· · ·O4 and O5· · ·O4a distances of 2.717, 2.680 and 2.710 Å, respectively. Moreover, two chains interact through more hydrogen bonds between the phthalate ligands and molecules of water (coordinated and noncoordinated), the O5· · ·O7a and O7· · ·O3 distances being 2.771 and 2.731 Å, respectively, generating a hydrophilic channel of 6.78 x 4.54 Å. Furthermore, molecular channels are maintained via π - π stacking of the phen ligands, with a distance between the centroids of 3.428 and 3.517 Å (cycles involving N1 atoms).

There are just three one-dimensional Mn^{II} compounds with only one $\mu_{1,3}$ carboxylate bridge and an anti–anti conformation reported in the literature [18,38] and one of them is a polymorph of the present compound, but with different structural parameters [18]. While the Mn - N distances are identical, the Mn - O distances are longer than in compound **6** (ca. 2.201 and 2.154 Å for the oxygen atoms of the phthalate ligands and water, respectively), which leads to a slightly longer Mn· · ·Mn distance (6.493 Å). However, the supramolecular architecture is analogous, the channel being larger (6.78 x 5.14 Å).

3.3. Magnetic properties

452   Magnetic susceptibility data were recorded for all compounds (1–6), from room

453   temperature to 2 K. $\chi_M T$ versus T and χ_M versus T plots for [{Mn(H$_2$O)(phen)}$_2$(μ-2-

454   COOHC$_6$H$_4$COO)$_2$ μ -O)](ClO$_4$)$_2$ (1) are shown in Fig. 8. At 300 K, the $\chi_M T$ value is 5.79

455   cm3 mol^{-1} K, close to the typical value for two uncoupled Mn^{III} ions (S = 2, 6 cm3 mol^{-1}

456   K). As the temperature descends, the v$_M$T values fall to 0.32 cm3 mol^{-1} K at 2 K, indicative

457   of an antiferromagnetic coupling (spin ground state S = 0). This is also clearly evidenced by

458   a maximum in the χ_M versus T plot at 0.17 cm3 mol^{-1} for T ~ 10 K (inset Fig. 8). The

459   experimental data were fitted by using the spin Hamiltonian H = -JS$_1$S$_2$ and the

460   corresponding susceptibility expression for two Mn^{III} ions with the same g value [39]. The

461   best fit of the $\chi_M T$ (χ_M) data corresponds to J = -3.7 (-3.5) cm^{-1}, g = 1.99 (1.99) and R =

462   5.2 x 10^{-4} (8.2 x 10^{-4}).

463   The magnetic interaction for this kind of complex is weak, with J values between 18

464   and –12 cm^{-1}, and may depend on different structural parameters [7–11,26–30,34]. A

465   magneto-structural study carried out for analogous compounds with different

466   orthosubstituted benzoato ligands analyzed the effect of three structural parameters: the

467   distortion of the coordination octahedron of the manganese ions (λ), the torsion angle

468   between the carboxylate group and the phenyl ring (ω) and the relative orientation of the

469   coordination octahedra (τ) [29]. According to this study, an antiferromagnetic interaction is

470   usually favored in compounds with a high k value (elongated distortion, $\lambda > 2$), big ω angles

471   and τ angles smaller than 100°. Table 7 gathers the magnetic coupling constants and selected

472   structural parameters for compounds with the formula [{Mn(L)(NN)}$_2$(μ-O)(μ -2-

473   RC$_6$H$_4$COO)$_2$]X$_2$. As can be seen, compound 1 shows $\lambda \sim 2.29$, $\omega \sim 23°$ and $\tau \sim 91°$, these

474   values corresponding to a weak antiferromagnetic interaction, as experimentally observed.

475   Interestingly, the analogous compound A, with the same R group, shows a ferromagnetic

476   coupling (J = 4.7 cm^{-1}) [10]. The main reason for this different magnetic behavior is the

477   counteranion; nitrate anions lead to more rhombic distortions around manganese ions,

478   especially if they are coordinated, favoring a ferromagnetic interaction.

479   The $\chi_M T$ versus T plot for [{Mn(phen)$_2$}$_2$(μ-O)$_2$](NO$_3$)$_3$ (**2**) is shown in Fig. S5. At

480   300 K, the $\chi_M T$ value is 0.64 cm^3 mol^{-1} K and this decreases sharply on cooling, reaching a

481   value of 0.38 cm^3 mol^{-1} K at 80 K. Below 10 K, the $\chi_M T$ values fall slightly to 0.35 cm^3

482   mol^{-1} K at 2 K, probably due to antiferromagnetic intermolecular interactions. This behavior

483   is typical for [Mn$_2$(μ -O)$_2$]$^{3+}$ systems, where the antiferromagnetic coupling between Mn^{III}

484   and Mn^{IV} ions is so strong that at room temperature the $\chi_M T$ value is much lower than the

485   expected for two uncoupled ions (S = 2 and S = 3/2, $\chi_M T$ = 4.875 cm^3 mol^{-1} K). The $\chi_M T$

486   value at low temperature is close to that expected for a ground spin state S = ½ ($\chi_M T$ = 0.375

487   cm^3 mol^{-1} K). The experimental data were fitted using the spin Hamiltonian H = -$JS1S2$ and

488   the corresponding susceptibility expression for a Mn^{III}Mn^{IV} system [39]. In order to fit the

489   whole curve, intermolecular interactions (zJ') were considered. The best fit was obtained

490   with J = -332.5 cm^{-1}, zJ' = -0.13 cm^{-1}, g = 2.03 and R = 4.85 x 10^{-5}. This J value agrees

491   with those reported for other [Mn$_2$(μ-O)$_2$]3+compounds, from -237 to -442 cm^{-1} [36,40],

492   the antiferromagnetic interaction being stronger than that for the analogous compounds

493   [{Mn(NN)$_2$}$_2$(μ -O)$_2$]X$_3$ with NN = bpy or phen, the J values ranging from -268 to -300

494   cm^{-1} [36].

495   Regarding Mn^{II} compounds, the magnetic results are classified according to the

496   nuclearity of the compounds. The $\chi_M T$ versus T and χ_M versus T plots for the dinuclear

497   compounds [{Mn(H$_2$O)(-phen)$_2$}$_2$(μ-4-COOC$_6$H$_4$COO)](NO$_3$)$_2$ (**3**) and [{Mn(phen)$_2$}$_2$(μ

498   -2-COOHC$_6$H$_4$COO)$_2$](ClO$_4$)$_2$ (**5**) are shown in Fig. 9. At 300 K, the $\chi_M T$ values are 8.56

499   and 8.68 cm^3 mol^{-1} K for compounds **3** and **5** respectively, close to the typical value for two

500   uncoupled Mn^{II} ions (S = 5/2, 8.75 cm^3 mol^{-1} K). As the temperature decreases, the $\chi_M T$

501   values for compound **5** fall to 0.91 cm^3 mol^{-1}K at 2K, which is indicative of an

502   antiferromagnetic coupling (spin ground state S = 0). This is also clearly evidenced by a

503   maximum in the χ_M versus T plot (inset Fig. 9) at 0.424 cm^3 mol^{-1} for $T \sim 7$ K. However,

504   for compound **3,** the $\chi_M T$ values remain almost constant as the temperature falls to 12 K and

505   then they decrease slightly to 7.91 cm^3 mol^{-1} K at 2 K.

506   The experimental data were fitted by using the spin Hamiltonian $H = -JS_1S_2$ and the

507   corresponding susceptibility expression for two Mn^{II} ions, assuming the same g value [39].

508   For compound **3**, the best fit of the $\chi_M T$ data corresponds to $J = -0.04$ cm^{-1}, g = 1.99 and R

509   = 7.4 x 10^{-6}. A J value this low agrees with the long Mn· · ·Mn distance (11.547 Å) provided

510   by the bis-monodentate bridging mode of the terephthalate ligand and is in the range -0.02

511   to -0.07 cm^{-1} found for Mn^{II} complexes with the same bridge [14,16a,17]. However, the

512   antiferromagnetic interaction observed could be due to intermolecular interactions, as the

513   Mn· · ·Mn distances are shorter (~9 Å). In this case, the Curie–Weiss model evaluates these

514   interactions at a θ value of -1.0 K. The analogous compound [{Mn(H$_2$O)(phen)$_2$}$_2$(μ-4-

515   COOC$_6$H$_4$COO)](ClO$_4$)$_2$ is reported in the literature, with a J value of -0.065 cm^{-1} [14].

516   The authors observed that if this compound was heated, the antiferromagnetic coupling

517   became stronger, the J value being -1.6 cm^{-1}. This increase was explained by a structural

518   change: a loss of the coordinated molecules of water and subsequent carboxylate bridging in

519   a *syn–syn* conformation. A similar study was carried out with compound **3**, heating to 400

520   K, but just a slight increase in the magnetic response was observed ($J = -0.06$ cm^{-1}, g = 2.02

521   and $R = 1.2$ x 10^{-5}). This different behaviour could be due to the existence of hydrogen bonds

522   between the coordinated water molecules, the nitrate anions and the carboxylate bridges,

523   which stabilize the complex and do not allow the loss of the water molecules.

524   The same Hamiltonian was used for compound **5**, the best fit of the $\chi_M T$ (χ_M) data

525   corresponding to $J = -1.5$ (-1.5) cm^{-1}, g = 2.00 (1.98) and $R = 2.1$ x 10^{-4} (1.7 x 10-4). These

526   J values agree with the range ~0 to -1.9 cm^{-1} found in the literature for other Mn^{II}

527   compounds with two *syn–anti* carboxylate bridges [13b,31b]. As has been indicated, there

528   are three compounds with the same core reported in the literature, but only one of them has

529   been magnetically characterized, showing a weaker antiferromagnetic coupling (J value of -

530   0.3 cm^{-1}) [13b].

Table 8 gathers the magnetic coupling constant and selected structural parameters for compounds with the formula $[\{Mn(NN)_2\}_2(\mu\text{-}2\text{-}RC_6H_4COO)_2]^{+2}$. As can be seen, all the compounds show weak antiferromagnetic coupling, the J values being very similar, except for compound e. As was mentioned, the torsion angle between the carboxylate group and the phenyl ring (ω) plays an important role in the magnetic properties of dinuclear Mn^{III} compounds, increasing the antiferromagnetic behavior. However, for these dinuclear Mn^{II} compounds this structural parameter has no affect since compounds **a** and **b** show the same J value whilst the torsion angle is very different. In these compounds the magnetic interaction pathway takes place through the carboxylate ligands, the small structural differences affecting the overlap between the lone-pair electrons of the oxygen atoms and the d orbitals of the Mn ions (Scheme 1). When comparing the structural data for compounds **5** and **e**, both with the same cationic complex, the main differences are the α and γ angles, an increase in these angles diminishes the antiferromagnetic contribution.

The $\chi_M T$ versus T and χ_M versus T plots for the 1D system $[Mn(\mu\text{-}2\text{-}COOC_6H_4COO)(H_2O)_2(phen)]_n$ (**6**) are shown in Fig. 10. At 300 K, the $\chi_M T$ value is 4.47 cm^3 mol^{-1} K, close to the typical value for one Mn^{II} ion (S = 5/2, 4.375 cm^3 mol^{-1} K). As the temperature decreases, the $\chi_M T$ values fall to 0.75 cm^3 mol^{-1}K at 2K, indicative of an antiferromagnetic interaction between the manganese ions in the chain. This behaviour is also observed in the χ_M versus T plot (inset Fig. 10) with a maximum at 0.389 cm^3 mol^{-1} for $T \sim 3.5$ K.

The magnetic susceptibility data were analyzed by the analytical expression, derived by Fisher [41] for an infinite chain of classical spins based on the Hamiltonian $H = -J\Sigma S_i \cdot S_{i+1}$, for local spin values of $S = 5/2$. The best fit of the $\chi_M T$ (χ_M) data corresponds to $J = -0.55$ (-0.56) cm^{-1}, $g = 2.04$ (2.05) and $R = 6.8$ x 10^{-6} (3.9 x 10^{-5}). As has been said, there are just three 1D compounds with one anti-anti carboxylate bridge; two of them have been magnetically characterized, the J values being -0.50 and -0.91 cm^{-1} [31b]. This bridging mode is also found in other Mn^{II} compounds, with J values in the range ~0 to 0.70 cm^{-1} [42].

559   The $\chi_M T$ versus T and M versus H plots for the 2D system [Mn$_3$(μ-4-

560   COOC$_6$H$_4$COO)$_3$(bpy)$_2$]$_n$ (**4**) are shown in Fig. 11. At 300 K, the $\chi_M T$ value is 12.72 cm^3

561   mol^{-1} K, close to the value of 13.125 cm^3 mol^{-1} K which corresponds to three uncoupled

562   Mn^{II} ions. When the temperature decreases, the $\chi_M T$ values fall to 4.45 cm^3 mol^{-1} K at 2 K,

563   very close to the expected value of 4.375 cm^3 mol^{-1} K for a spin ground state $ST = 5/2$ and

564   g = 2, indicative of an antiferromagnetic coupling. This spin value is confirmed by the field

565   dependence of the magnetization at 2 K, which shows an $M/N\mu b$ saturation value indicative

566   of five unpaired electrons (inset Fig. 11).

567   Taking into account that this 2D system consists of trinuclear units bridged by

568   terephthalate ligands, it can be considered that the magnetic response observed is mainly due

569   to the interaction in the trinuclear entity. Based on Kambe's vector coupling scheme [43],

570   the spin Hamiltonian considered would be $H = -J(S_1 S_2 + S_2 S_3) - J_{13}(S_1 S_3)$, where it is

571   assumed that $J12 = J13 = J$ (Scheme 2). As the distance between the terminal manganese

572   ions in the linear complex is large, their magnetic interaction is negligible ($J_{13} = 0$) and just

573   the Mn$_1$· · ·Mn$_2$ and Mn$_2$·· · ·Mn$_3$ interactions (J) are considered. The expression for the

574   magnetic susceptibility of three linear Mn^{II} ions is obtained from the Van Vleck formula

575   [39]. The best fit of experimental data corresponds to $J = -4.5$ cm^{-1}, $g = 2.02$ and $R = 5.8$ x

576   10^{-5}.

577   The antiferromagnetic interaction for compound **4** is stronger than that reported for

578   analogous 2D systems [16a–c], although the J value agrees with those from –6.6 to – 2.1

579   cm^{-1} reported in the literature for linear Mn^{II} trinuclear compounds [31a,37a]. For this kind

580   of compound, the magnetic interaction between the manganese ions takes place through two

581   μ $_{1,3}$-carboxylate bridges with a *syn–syn* coordination mode and a μ $_{1,1}$-carboxylate bridge,

582   which is the main antiferromagnetic interaction pathway. It depends on the Mn-O$_b$-Mn

583   angle, but also in the existence of an additional contribution from the μ $_{1,3}$-carboxylate

584   bridge with a *syn–anti* coordination mode, which has been reported to decrease the

585   antiferromagnetic interaction [31a]. Table 9 collects selected structural parameters and J

586   values for the three 2D systems, Scheme 3 showing the distances involved. Compound **4**

587   shows a quite symmetric $\mu_{1,1}$ bridge and a large Mn-O$_d$ distance, the $\mu_{1,3}$ character being

588   small. However, for compound **Y**, which also shows a symmetric bridge, the Mn-O$_d$ distance

589   is shorter, which leads to a $\mu_{1,3}$ contribution and a decrease in the antiferromagnetic

590   interaction, as experimentally observed. For compound **Z**, a $\mu^1{}_{,3}$ contribution is also

591   expected.

592

593   *3.4. EPR spectra*

594   EPR spectra of Mn^{II} compounds **3–6** were recorded on powdered samples at different

595   temperatures. At room temperature, all of them show a band centred at g ~ 2, however, at 4

596   K, the spectrum of each compound is noticeably different and allows for identification of

597   each kind of complex.

598   The EPR spectra of compounds **3** and **5** at 4 K are very different, although both are

599   dinuclear systems (Fig. 12). For compound **3**, the main band is wider and shifted towards g

600   ~ 2.2, showing another band at lower fields (g ~ 4.5). In this compound the manganese ions

601   are bridged by one terephthalate ligand and the magnetic coupling is so weak that the two

602   manganese ions are practically isolated and the spectrum would correspond to that expected

603   for a system with $S = 5/2$. For compound **5**, the strong signal is centred at g ~ 2 and there are

604   two more bands at both sides and other features at lower fields. The manganese ions in this

605   compound are bridged by two $\mu_{1,3}$ carboxyalate ligands and a significant antiferromagnetic

606   interaction is observed, the spin ground state being $S = 0$. At 4 K it should be EPR silent,

607   however, the small J value (-1.5 cm^{-1}) allows the lowest excited states $S = 1$ and $S = 2$ to be

608   populated.

609   Both spectra at 4 K were simulated with the easyspin software [21] by considering a

610   mononuclear system with $S = 5/2$ for compound **3** and a dinuclear system of two $S = 5/2$ ions

611   for compound **5**, including a magnetic exchange interaction (J) obtained from the magnetic

612   data. In both cases, the axial and rhombic zero-field splitting (ZFS) parameters of the single

613   ion (D_{Mn} and E_{Mn}) were included. Fairly good simulations were achieved with D_{Mn} and

614   E_{Mn} values of 0.090 and 0.023 cm^{-1} for compound **3** and 0.090 and 0.020 cm^{-1} for

compound **5**. These values agree with the small distortions characteristic of Mn^{II} ions and are similar to those reported for analogous compounds [31b].

The EPR spectrum of the 2D system **4** is very sensitive to temperature (Fig. S6). The broad band centred at $g \sim 2$, observed at room temperature, decreases in intensity on lowering the temperature and, at 4 K, the most intense signal is found at low field ($g \sim 4$), with some other features at high field. This behaviour is characteristic of trinuclear compounds and, as has been seen before, this compound can be considered as isolated trinuclear entities from a magnetic point of view, the spin ground state being $S_T = 5/2$, with the first excited state ($S_T = 3/2$) at $-3J/2$ above it. Therefore, with $J = -4.5$ cm^{-1}, at 4 K only the ground state may be populated and the spectra corresponds to a system with $S = 5/2$ with ZFS.

The spectrum at 4 K was simulated by considering an isolated spin state $S = 5/2$ with axial and rhombic zero-field splitting. The ZFS parameters obtained from this simulation therefore correspond to the ground state, $D_{5/2}$ and $E_{5/2}$ and depend on the ZFS parameters of the interacting ions, D_{Mn} and E_{Mn}, and dipolar and anisotropic interactions between the ions. A correct simulation was achieved with $D_{5/2} = 0.17$ cm^{-1} and $E_{5/2} = 0.05$ cm^{-1} (Fig.13). These values agree with those reported for trinuclear compounds [37a].

The EPR spectrum of the 1D system **6** shows a single band centred at $g \sim 2$ that widens on decreasing the temperature (Fig. S7). The peak-to-peak linewidth changes from 120 G at 77 K to 157 G at 4 K. The same behaviour was observed for analogous compounds reported in the literature [37a]. This broadening on lowering the temperature may be explained by considering the main factors that influence the linewidth for an isotropic Heisenberg 1D system [44]. When the superexchange interactions along the chain are the predominant effect, a narrowing of the signal is observed, while when the dipolar interactions are more important, a broadening of the signal is observed, as in compound **6**, with a very weak antiferromagnetic coupling ($J = -0.55$ cm^{-1}). Moreover, for Mn^{II} 1D systems, there are additional broadening mechanisms, such as hyperfine coupling and single-ion ZFS effects.

3.5. Catalase activity

Several dinuclear Mn^{III} compounds analogous to **1** and **A** have been shown to catalyse the disproportion reaction of H_2O_2 into H_2O and O_2 [7–9]. For this kind of compound, the catalase activity depends on quite a few factors, such as the electronic character of the substituent or the counteranion. In this work, the catalytic activity of Mn^{III} compounds and also that of Mn^{II} systems has been analysed. All compounds studied are stable under aerobic conditions. The Mn^{III} compounds are completely soluble in CH_3CN, leading to brown solutions, while some Mn^{II} compounds are only partially soluble, forming pale yellow suspensions. In order to analyze the catalytic activity of these compounds with H_2O_2 and the effect of the substrate concentration on the reaction rate and efficiency, three experiments were carried out adding different amounts of H_2O_2 30 % (0.50, 0.60 and 0.70 mL), which correspond to $[H_2O_2]/[compound]$ ratios of 1224, 1470 and 1714.

The dinuclear Mn^{III} compounds **1** and **A** show a very low activity since after 10 min of reaction only ~30 mol of H_2O_2 per mol of catalyst are decomposed (~2%), whatever the experiment, and the reaction does not last much longer. The reaction with H_2O_2 should present two steps. The initial stoichiometric reduction of the dinuclear Mn^{III} complex leads to the formation of a small amount of O_2 and then there is a catalytic cycle between Mn^{II}/Mn^{III} intermediates. Despite the O_2 evolved corresponding to 30 catalytic cycles, these results are worse than those reported for other dinuclear Mn^{III} compounds with n-RC_6H_4COO bridges (R = Cl, CH_3, F), where the lowest catalytic activity observed corresponded to 20% H_2O_2 being decomposed [8]. Thus, comparatively, these two compounds are practically inactive, despite having a similar structure. Compounds **1** and **A** show COOH groups placed in *ortho* positions and from an electronic point of view, they can be compared to compounds with a Cl group, a similar behavior being expected. However, the presence of COOH groups could affect the hydrogen bonds with the substrate and/or counteranions, or generate steric hindrance making the approach of H_2O_2 difficult.

Mn^{II} compounds show better catalase activities than dinuclear Mn^{III} compounds. In this case, the first step is the reduction of H_2O_2 to H_2O and the formation of Mn^{III} catalytic species, which enter the catalytic cycle generating O_2. Compound **3** reaches ~800 mol of H_2O_2 decomposed per mol of catalyst after one hour of reaction. In this compound, each manganese ion shows one labile position occupied by a water molecule, which could be replaced by H_2O_2, and the monodentate terephthalate ligand could help in the protons transfer.

For compound **4**, the plot of O_2 evolved versus time, shown in Fig. 14, indicates that after 10 min of reaction a new catalytic species may form, as the rate of oxygen evolved increases, reaching ~500 mol of H_2O_2 per mol of catalyst. There is no labile position on the manganese ions in this case; thus a low activity would be expected. The most suitable position for the coordination of H_2O_2 would be one of the terminal manganese ions, the de-coordination of one oxygen atom of one carboxylate ligand being needed. In this case, the longest Mn-O distance corresponds to the oxygen atom which does not take part in the bridging to the central manganese ion (O2 in Fig. 5). During the reaction of compound **4**, a white product was formed, which corresponds to manganese (II) terephthalate. This is proof of the structural change suggested by the shape of the curves shown in Fig. 14 and could be the new catalytic species. However, its catalase activity was investigated and this complex is inactive. Therefore, the partial decomposition of the catalyst generates a new catalytic species soluble in CH_3CN.

Compounds **5** and **6** show lower catalytic activities and are very similar in the three experiments; after 30 min of reaction only ~140 mol of H_2O_2 per mol of catalyst are decomposed. For compound **5**, there is no labile position on the manganese ion for the coordination of H_2O_2, the de-coordination of one oxygen atom of one carboxylate bridge being necessary to start the reaction. However, for compound **6**, there are two positions occupied by water molecules and the catalase activity is low as well. The crystal structure of this compound shows several intra and intermolecular hydrogen bonds leading to channels; their possible conservation in solution could explain the low catalytic activity. On the other

hand, as in compounds **1** and **A**, the presence of a COO group in an *ortho* position could make the reaction difficult.

Although the structures of these compounds are not analogous and a comparison of their activity should be taken carefully, the fact is that compounds with phthalate ligands (**1**, **5** and **6**) show worse catalase activity than compounds with terephthalate ligands (**3** and **4**).

4. CONCLUSION

Carboxybenzoate ligands (phthalate, isophthalate and terephthalate) behave differently from other benzoate derivative ligands since analogous reactions do not give rise to the same type of compound as had been seen until now. The crystal structure analyses show the trend of phthalate ligands to coordinate using only one carboxylate group while terephthalate ligands use both of them. MnII compounds can be distinguished by their EPR spectra at 4 K. All the compounds studied show low catalase activity, this activity being higher for compounds with terephthalate ligands. Contrary to previous studies for analogous compounds, dinuclear MnIII compounds **1** and **A** are practically inactive.

ACKNOWLEDGEMENTS

6. REFERENCES

[1]   M. Murrie, D.J. Price, Annu. Rep. Prog. Chem. Sect. A 103 (2007) 20. And references cited therein.

[2]   C.S. Mullins, V.L. Pecoraro, Coord. Chem. Rev. 252 (2008) 416.

[3]   (a) A.J. Wu, J.E. Penner-Hahn, V.L. Pecoraro, Chem. Rev. 104 (2004) 903; (b) S. Signorella, C. Hureau, Coord. Chem. Rev. 256 (2012) 1229.

[4]   (a) V.V. Barynin, M.M. Whittaker, S.V. Antonyuk, V.S. Lamzin, P.M. Harrison, P.J. Artymiuk, J.W. Whittaker, Structure 9 (2001) 725; (b) S.V. Antonyuk, V.R. Melik-Adamyan, A.N. Popov, V.S. Lamzin, P.D. Hempstead, P.M. Harrison, P.J. Artymyuk, V.V. Barynin, Crystallogr. Rev. (Transl. Kristallografiya) 45 (2000) 105; (c) V.V. Barynin, P.D. Hempstead, A.A. Vagin, S.V. Antonyuk, W.R. Melik-Adamyan, V.S. Lamzin, P.M. Harrison, P.J. Artymiuk, J. Inorg. Biochem. 67 (1997) 196.

[5]   S.V. Khangulov, V.V. Barynin, S.V. Antonyuk-Barynina, Biochim. Biophys. Acta 1020 (1990) 25.

[6]   G.S. Waldo, J.E. Penner-Hahn, Biochemistry 34 (1995) 1507.

[7]   G. Fernandez, M. Corbella, M. Alfonso, H. Stoeckli-Evans, I. Castro, Inorg. Chem. 43 (2004) 6684.

[8]   M. Corbella, G. Fernandez, P. Gonzalez, M.A. Maestro, M. Font-Bardia, H. Stoeckli-Evans, Eur. J. Inorg. Chem. (2012) 2203.

[9]   V. Gómez, M. Corbella, Eur. J. Inorg. Chem. (2012) 3147.

[10] C. Chen, H. Zhu, D. Huang, T. Wen, Q. Liu, D. Liao, J. Cui, Inorg. Chim. Acta 320 (2001) 159.

[11] L.F. Jones, A. Prescimone, M. Evangelisti, E.K. Brechin, Chem. Commun. (2009) 2023.

[12] (a) C. Chen, D. Huang, X. Zhang, F. Chen, H. Zhu, Q. Liu, D. Liao, L. Li, L. Sun, Inorg. Chem. 42 (2003) 3540; (b) G.-Y. An, A.-L. Cui, H.-Z. Kou, Inorg. Chem. Commun. 14 (2011) 1475.

[13] (a) J.-M. Yang, Z.-H. Zhou, H. Zhang, H.-L. Wan, S.-J. Lu, Inorg. Chim. Acta 358

(2005) 1841; (b) C. Ma, W. Wang, X. Zhang, C. Chen, Q. Liu, H. Zhu, D. Liao, L. Li, Eur. J. Inorg. Chem. (2004) 3522.

[14] J. Cano, G. De Munno, J.L. Sanz, R. Ruiz, J. Faus, F. Lloret, M. Julve, A.J. Caneschi, J. Chem. Soc., Dalton Trans. (1997) 1915.

[15] (a) Y.-S. Yang, W. Gu, L.-Z. Zhang, F.-X. Gao, S.-P. Yan, J. Coord. Chem. 60 (2007) 1913; (b) A. Escuer, F.A. Mautner, N. Sanz, R. Vicente, Inorg. Chim. Acta 340 (2002) 163.

[16] (a) X.-M. Lu, P.-Z. Li, X.-T. Wang, S. Gao, X.-J. Wang, S. Wang, Y.-H. Deng, Y.-J. Zhang, L. Zhou, Polyhedron 27 (2008) 2402; (b) W.-Z. Zhang, Q. Xu, Acta Crystallogr., Sect. E: Struct. Rep. Online 64 (2008) m995; (c) Z.-Q. Jiang, Z. Zhao, G.-Y. Jiang, D.-C. Hou, Y. Kang, Inorg. Chem. Commun. 14 (2011) 1975.

[17] (a) C.S. Hong, J.H. Yoon, Y.S. You, Inorg. Chim. Acta 358 (2005) 3341; (b) S.C. Manna, S. Konar, E. Zangrando, K. Okamoto, J. Ribas, N.R. Chaudhuri, Eur. J. Inorg. Chem. (2005) 4646.

[18] Y. Zhang, L. Jianmin, Z. Min, Q. Wang, X. Wu, Chem. Lett. (1998) 1051.

[19] (a) M. Devereux, M. McCann, V. Leon, M. Geraghty, V. McKee, J. Wikaira, Met.-Based Drugs 7 (2000) 275; (b) Z.-H. Jian, S.-L. Ma, D.-Z. Liao, S.-P. Yan, G.-L. Wang, X.-K. Yao, R.-J. Wang, Chem. Commun. (1993) 745; (c) C. Ma, C. Chen, Q. Liu, D. Liao, L. Li, L. Sun, New. J. Chem. 27 (2003) 890; (d)N.L. Rosi, J. Kim, M. Eddaoudi, B. Chen, M. O'Keeffe, O.M. Yaghi, J. Am. Chem. Soc. 127 (2005) 1504; (d) C.-S. Liu, S.-R. Li, C.-Y. Li, J.-J. Wang, X.-H. Bu, Inorg. Chim. Acta 360 (2007) 2532; (e) D. Sun, R. Cao, Y. Liang, W. Shi, W. Su, M. Hong, J. Chem. Soc., Dalton Trans. (2001) 2335; (f) L. Zhang, S.Y. Niu, J. Jin, L.-P. Sun, G.-D. Yang, L. Ye, Inorg. Chim. Acta 362 (2009) 1448; (g) C.S. Hong, W. Do, Inorg. Chem. 36 (1997) 5684; (h) F. Luo, Y.-X. Che, J.M. Zheng, Inorg. Chem. Commun. 11 (2008) 358.

[20] T. Sala, M.V. Sargenti, J. Chem. Soc., Chem. Comm. (1978) 253.

[21] J.A. Kaduk, Acta Crystallogr., Sect. B: Struct. Sci. 58 (2002) 815.

[22] S. Stoll, A. Schweiger, J. Magn. Reson. 178 (2006) 42.

[23] G.M. Sheldrick, Acta Crystallogr. A 64 (2008) 112.

796 [24] G. M. Sheldrick, SHELX-TL, Bruker AXS Inc., Madison, Wisconsin, USA.

797 [25] A. Altomare, M.C. Burla, M. Camalli, G.L. Cascarano, C. Giacovazzo, A. Guagliardi,
798   A.G.G. Moliterni, G. Polidori, R. Spagna, J. Appl. Crystallogr. 32 (1999) 115.

799 [26] G. Fernández, M. Corbella, G. Aullón, M.A. Maestro, J. Mahía, Eur. J. Inorg. Chem.
800   (2007) 1285.

801 [27] M. Corbella, V. Gómez, B. Garcia, E. Rodríguez, B. Albela, M.A. Maestro, Inorg.
802   Chim. Acta 376 (2011) 456.

803 [28] V. Gómez, M. Corbella, G. Aullón, Inorg. Chem. 49 (2010) 1471.

804 [29] V. Gómez, M. Corbella, O. Roubeau, S.J. Teat, Dalton Trans. 40 (2011) 11968.

805 [30] B. Albela, M. Corbella, J. Ribas, Polyhedron 15 (1996) 91.

806 [31] (a) V. Gómez, M. Corbella, Eur. J. Inorg. Chem. (2009) 4471; (b) V. Gómez, M.
807   Corbella, M. Font-Bardia, T. Calvet, Dalton Trans. 39 (2010) 11664; (c) B. Albela, M.
808   Corbella, J. Ribas, I. Castro, J. Sletten, H. Stoeckli-Evans, Inorg. Chem. 37 (1998)
809   788; (d) G. Fernandez, M. Corbella, J. Mahia, M.A. Maestro, Eur. J. Inorg. Chem. 9
810   (2002) 2502; (e) V. Gómez, M. Corbella, J. Chem. Crystallogr. 41 (2011) 843.

811 [32] B. Deacon, R.J. Phillips, Coord. Chem. Rev. 33 (1980) 227.

812 [33] (a) B.C. Dave, R.S. Czernuszewickz, Inorg. Chim. Acta 281 (1998) 25; (b) R. Ruiz,
813   C. Sangregorio, A. Caneschi, P. Rossi, A.B. Gaspar, J.A. Real, M.C. Muñoz, Inorg.
814   Chem. Commun. 3 (2000) 361; (c) K.R. Reddy, M.V. Rajasekharan, S. Sukumar,
815   Polyhedron 15 (1996) 4161; (d) T. Tanase, S.J. Lippard, Inorg. Chem. 34 (1995) 4682;
816   (e) U. Bossek, K. Wieghardt, K. Nuber, J. Weiss, Inorg. Chim. Acta 165 (1989) 123;
817   (f) S.K. Mandal, W.H. Armstrong, Inorg. Chim. Acta 229 (1995) 261; (g)A.G.
818   Blackman, J.C. Huffman, E.B. Lobkovsky, G. Christou, J. Chem. Soc., Chem.
819   Commun. 2 (1991) 989; (g) H.J. Mok, J.A. Davis, S. Pal, S.K. Mandal, W.H.
820   Armstrong, Inorg. Chim. Acta 263 (1997) 385; (h) J.W. de Boer, J. Brinksma, W.R.
821   Browne, A. Meetsma, P.L. Alsters, R. Hage, B.L. Feringa, J. Am. Chem. Soc. 127
822   (2005) 7990; (i) R. Hage, E.A. Gunnewegh, J. Niel, F.S.B. Tjan, T. Weyhermuller, K.
823   Wieghardt, Inorg. Chim. Acta 268 (1998) 43; (j) V.B. Romakh, B. Therrien, L.
824   Kamazin-Brelot, G. Labat, H. Stoeckli-Evans, G.B. Shulpin, G. Suss-Fink, Inorg.
825   Chim. Acta 359 (2006) 1619; (k) J.W. de Boer, P.L. Alsters, A. Meetsma, R. Hage,

826   W.R. Browne, B.L. Feringa, Dalton Trans. (2008) 6283; (l) J. Li, S. Yang, F. Zhang,
827   Z. Tang, Q. Shi, Z. Zhou, Chin. Sci. Bull. 45 (2000) 1079.

828   [34]   (a) M. Corbella, R. Costa, J. Ribas, P.H. Fries, J.M. Latour, L. Ohrstrom, X. Solans,
829   V. Rodríguez, Inorg. Chem. 35 (1996) 1857; (b) J.B. Vincent, H.L. Tsai, A.G.
830   Blackman, S. Wang, P.D. Boyd, K. Folting, J.C. Huffman, E.B. Lobkovsky, D.N.
831   Hendrickson, G. Christou, J. Am. Chem. Soc. 115 (1993) 12353; (c) K. Mitra, D.
832   Mishra, S. Biswas, C.R. Lucas, B. Adhikary, Polyhedron 25 (2006) 1681; (d) C.
833   Cañada-Vilalta, W.E. Streib, J.C. Huffmann, T.A. O'Brian, E.R. Davidson, G.
834   Christou, Inorg. Chem. 43 (2004) 101; (e) K. Wieghardt, U. Bossek, D. Ventur, J.
835   Weiss, J. Chem. Soc. Chem. Commun. (1985) 347; (f) K. Wieghardt, U. Bossek, B.
836   Nuber, J. Weiss, J. Bonvoisin, M. Corbella, S.E. Vitols, J.J. Girerd, J. Am. Chem. Soc.
837   110 (1988) 7398; (g) C. Bolm, N. Meyer, G. Raabe, T. Weyhermüller, E. Bothe, Chem.
838   Commun. (2000) 2435; (h) J.E. Sheats, R.S. Czernuszewicz, G.C. Dismukes, A.L.
839   Rheingold, V. Petrouleas, J.A. Stubbe, W.H. Armstrong, R.H. Beer, S.J. Lippard, J.
840   Am. Chem. Soc. 109 (1987) 1435; (i) F.J. Wu, D.D. Kurtz Jr., K.S. Hagen, P.D.
841   Nyman, P.G. Debrunner, V.A. Vankai, Inorg. Chem. 29 (1990) 5174; (j) S. Ménage,
842   J.J. Girerd, A. Gleizes, J. Chem. Soc., Chem. Commun. (1988) 431.

843   [35]   (a) D. Ramalakshmi, M.V. Rajasekharan, Acta Crystallogr., Sect. B: Struct. Sci. 55
844   (1999) 186; (b) C. Wilson, F.K. Larsen, B.N. Figgis, Acta Crystallogr., Sect. C: Cryst.
845   Struct. Commun. 54 (1998) 1797; (c) R. Manchanda, G.W. Brudvig, S. de Gala, R.H.
846   Crabtree, Inorg. Chem. 33 (1994) 5157.

847   [36]   (a) A.F. Jensen, Z. Su, S.K. Hansen, F.K. Larsen, Inorg. Chem. 34 (1995) 4244; (b)
848   M. Stebler, A. Ludi, H.-B. Burgi, Inorg. Chem. 25 (1986) 4743; (c) P.M. Plaksin, R.C.
849   Stoufer, M. Matthew, G.J. Palenik, J. Am. Chem. Soc. 94 (1972) 2121; (d) S.R.
850   Cooper, G.C. Dismukes, M.P. Klein, M. Calvin, J. Am. Chem. Soc. 100 (1978) 7248.

851   [37]   (a) X.-M. Lu, P.-Z. Li, X.-T. Wang, S. Gao, X.-J. Wang, L. Zhou, C.-S. Liu, X.-N.
852   Sui, J.-H. Feng, Y.-H. Deng, Q.-H. Jin, J. Liu, N. Liu, J.-P. Lian, Polyhedron 27 (2008)
853   3669; (b) D. Kalita, R. Sara, J.B. Baruah, Inorg. Chem. Commun. 12 (2009) 569; (c)
854   R. Wortmann, U. Flörke, B. Sarkar, V. Umamaheshwari, G. Gescheidt, S. Herres-
855   Pawlis, G. Henkel, Eur. J. Inorg. Chem. (2011) 121.

856   [38]   (a) M.J. Baldwin, J.W. Kampf, M.L. Kirk, V.L. Pecoraro, Inorg. Chem. 34 (1995)
857   5252; (b) E. Colacio, J.M. Domínguez-Vera, M. Ghazi, R. Kivekäs, M. Klinga, J.M.

Moreno, Eur. J. Inorg. Chem. (1999) 441.

[39] J.H. Van Vleck, The Theory of Electric and Magnetic Susceptibilities, Oxford University Press, London, 1932.

[40] (a) C. Hureau, G. Blondin, M. Cesario, S. Un, J. Am. Chem. Soc. 125 (2003) 11637; (b) O. Horner, M.-F. Charlot, A. Boussac, E. Anxolabehere-Mallart, L. Tchertanov, J. Ghilhem, J.-J. Girerd, Eur. J. Inorg. Chem. (1998) 721; (c) J. Glerup, P.A. Goodson, A. Hazell, R. Hazell, D.J. Hodgson, C.L. McKenzie, K. Michelsen, U. Rychlewska, H. Toftlund, Inorg. Chem. 33 (1994) 4105; (d) P.A. Goodson, D.J. Hodgson, D.J. Michelsen, K. Inorg, Chim. Acta 172 (1990) 49; (e) A.R. Oki, J. Glerup, D.J. Hodgson, Inorg. Chem. 29 (1990) 2435; (f) P.A. Goodson, D.J. Hodgson, J. Glerup, K. Michelsen, H. Weihe, Inorg. Chim. Acta 197 (1992) 141; (g) Y.-M. Frapart, A. Boussac, R. Albach, E. Anxolabehere-Mallart, M. Delroisse, J.-B. Verlhac, G. Blondin, J.-J. Girerd, J. Guilhem, M. Cesario, A.W. Rutherford, D. Lexa, J. Am. Chem. Soc. 118 (1996) 2669.

[41] M.E. Fisher, Am. J. Phys. Rev. A 32 (1964) 343.

[42] (a) S. Sain, T.K. Maji, G. Mostafa, T.-H. Lu, N.R. Chaudhuri, Inorg. Chim. Acta 351 (2003) 12; (b) C. Hureau, S. Blanchard, M. Nierlich, G. Blain, E. Rivière, J.-J. Girerd, E. Anxolabéhère-Mallart, G. Blondin, Inorg. Chem. 43 (2004) 4415; (c) X.-M. Chen, Y.-X. Tong, Z.-T. Xu, T.C.W. Mak, J. Chem. Soc., Dalton Trans. (1995) 4001; (d) M.-X. Li, G.-Y. Xie, S.-L. Jin, Y.-D. Gu, M.-Q. Chen, J. Liu, Z. Xu, X.-Z. You, Polyhedron 15 (1996) 535.

[43] K. Kambe, J. Phys. Soc. Jpn. 5 (1950) 48.

[44] A. Bencini, D. Gatteschi, Electron Paramagnetic Resonance of Exchange Coupled Systems, Springer-Verlag, Berlin, Heidelberg, 1990.

884 **Table 1** Crystallographic data for compounds 1–6.

885

Complex	$1 \cdot 0.6CH_3CN \cdot 2H_2O$	$2 \cdot 2\text{-COOH-} C_6H_4COOH \cdot CH_3CN$	$3 \cdot 2CH_3CH_2OH$	$4 \cdot 0.75DMF \cdot 0.25H_2O$	$5 \cdot 3CHCl_3 \cdot 4H_2O$	$6 \cdot H_2O$
Chemical formula	$C_{41.2}H_{35.8}Cl_2Mn_2N_{4.6}O_{21}$	$C_{60}H_{44}Mn_2N_{13}O_{15}$	$C_{60}H_{52}Mn_2N_{10}O_{14}$	$C_{46.25}H_{33.75}Mn_3 N_{4.75}O_{13}$	$C_{67}H_{53}Cl_{11}Mn_2N_8O_{20}$	$C_{20}H_{18}MnN_2O_7$
Formula weight	1112.12	1296.96	1247.0	1028.85	1790.0	453.30
T (K)	100(2)	150(2)	100(2)	100(2)	105(2)	100(2)
λ (Mo Kα) (Å)	0.77490	0.75150	0.7749	0.71073	0.71073	0.71073
Crystal system	triclinic	triclinic	monoclinic	monoclinic	triclinic	monoclinic
Space group	$P\bar{1}$	$P\bar{1}$	$P2_1/c$	$C2/c$	$P\bar{1}$	$P2_1/c$
Crystal size (mm^3)	$0.10 \times 0.09 \times 0.03$	$0.22 \times 0.10 \times 0.06$	$0.15 \times 0.04 \times 0.04$	$0.30 \times 0.23 \times 0.14$	$0.2 \times 0.1 \times 0.1$	$0.35 \times 0.26 \times 0.13$
a (Å)	10.8607(6)	11.465(2)	9.5715(14)	18.3728(17)	15.640(5)	6.4197(11)
b (Å)	13.1213(8)	14.118(3)	12.8309(19)	25.544(2)	16.158(4)	14.0261(14)
c (Å)	18.3407(11)	18.504(4)	22.654(3)	9.8583(13)	17.171(5)	21.434(3)
α (°)	71.9950(10)	77.20(3)	90	90	86.84(2)	90
β (°)	86.0300(10)	79.64(3)	94.089(2)	90.669(14)	74.71(2)	99.429(14)
γ (°)	74.5740(10)	69.79(3)	90	90	65.41(2)	90
V (Å^3)	2395.9(2)	2723.3(10)	2775.1(7)	4626.2(8)	3798.7(19)	1903.9(5)
Z	2	2	2	4	2	4
ρ_{calc} (g cm^{-3})	1.542	1.582	1.492	1.477	1565	1.581
μ (mm^{-1})	0.909	0.635	0.67	0.876	0.795	0.741
$F(000)$	1134	1330	1288	2094	1816	935
θ range (°)	2.97–33.62	2.16–28.01	2.90–33.62	1.37–26.37	1.39–30.89	1.74–25.29
Index ranges	$15 \leqslant h \leqslant 15$	$0 \leqslant h \leqslant 14$	$-13 \leqslant h \leqslant 13$	$-22 \leqslant h \leqslant 22$	$-22 \leqslant h \leqslant 22$	$-7 \leqslant h \leqslant 7$
	$-18 \leqslant k \leqslant 18$	$-16 \leqslant k \leqslant 17$	$-18 \leqslant k \leqslant 18$	$-20 \leqslant k \leqslant 31$	$-22 \leqslant k \leqslant 20$	$-16 \leqslant k \leqslant 16$
	$-26 \leqslant l \leqslant 26$	$-22 \leqslant l \leqslant 23$	$-32 \leqslant l \leqslant 32$	$-12 \leqslant l \leqslant 12$	$-23 \leqslant l \leqslant 24$	$-25 \leqslant l \leqslant 25$
Measured reflections	35 445	10489	52 260	13359	33 223	6833
Independent reflections	14378	10489	8466	4688	18297	3458
Goodness-of-fit on F^2	1.049	1.061	1.019	1.044	0.926	1.051
Largest difference in peak and hole / eÅ^{-3}	1.298, −1.146	0.501, −0.583	0.371, −0.447	1.169, −0.415	0.737, −0.435	0.298, −0.267
$R_1{}^a$, wR$_2{}^b$ [I > 2σ(I)]	0.0617, 0.1586	0.0370, 0.1031	0.0509, 0.1256	0.0504, 0.1216	0.0511, 0.1261	0.0498, 0.1091

^{a} $R1 = \sum||F_o| - |F_c||/\sum|F_o|$.
^{b} $wR2 = \{\sum[w(F_o{}^2 - F_c{}^2)^2]/\sum[w(F_o{}^2)^2]\}^{1/2}$, $w = 1/[\sigma^2(F_o{}^2) + (aP)^2 + bP]$, $P = [(F_o{}^2) + 2F_c{}^2]/3$.

886

887

888

889   **Table 2.** Selected bond lengths (Å) and angles (°) for compound 1.

890

Mn1−O1	1.7898(19)	Mn2−O1	1.7924(19)
Mn1−N1	2.071(2)	Mn2−N4	2.071(2)
Mn1−N2	2.080(2)	Mn2−N3	2.065(2)
Mn1−O2	1.9574(18)	Mn2−O7	1.9593(18)
Mn1−O6	2.1818(19)	Mn2−O3	2.1843(17)
Mn1−O10	2.211(2)	Mn2−O11	2.2530(19)
Mn1···Mn2	3.1514(6)	Mn1−O1−Mn2	123.22(10)
O1−Mn1−N1	171.76(8)	O1−Mn2−N4	170.50(8)
O2−Mn1−N2	169.04(9)	O7−Mn2−N3	167.48(9)
O6−Mn1−O10	170.83(8)	O3−Mn2−O11	174.31(8)
O6−C9−C10−C15	41.56(35)	O3−C1−C2−C7	4.33(36)
C10−C15−C16−O9	52.44(40)	C2−C7−C8−O5	91.27(30)
O10−Mn1−Mn2−O11	91.33(9)		

891

892

893

894

895

896

897

898

899

900

901

902   **Table 3** Selected bond lengths (Å) and angles (°) for compound 3.

903

Mn1−O1	2.1195(11)	Mn1−N4	2.2665(12)
Mn1−N3	2.2930(12)	Mn1···Mn1a	11.517(6)
Mn1−O3	2.1194(12)	O1−Mn1−N3	162.00(4)
Mn1−N1	2.2575(13)	O3−Mn1−N1	160.01(5)
Mn1−N2	2.2690(12)	N2−Mn1−N4	161.05(4)

904   Symmetry codes: (a) −x, 1 − y, 1 − z.

905

906

907

908 **Table 4** Selected bond lengths (Å) and angles (°) for compound 4.

909

Mn1–O1	2.1946(18)	Mn1···Mn2	3.5260(7)
Mn1–O2	2.3888(18)	Mn1–Mn2–Mn1a	180.00(1)
Mn1–O3	2.1073(18)	N1–Mn1–O1	152.16(7)
Mn1–O6	2.0943(18)	N2–Mn1–O6	160.36(8)
Mn1–N1	2.232(2)	O2–Mn1–O3	149.10(7)
Mn1–N2	2.288(2)	O1–Mn2–O1a	179.99(6)
Mn2–O1	2.2057(16)	O4–Mn2–O4a	180.00(7)
Mn2–O4	2.1340(18)	O5–Mn2–O5a	180.00(7)
Mn2–O5	2.1136(18)	Mn1–O1–Mn2	106.51(7)

Symmetry codes: (a) $1/2 - x$, $1/2 - y$, $1 - z$.

910

911

912

913

914 **Table 5** Selected bond lengths (Å) and angles (°) for compound 5.

915

Mn1−O6	2.136(2)	Mn2−O2	2.141(2)
Mn1−N3	2.312(2)	Mn2−N7	2.303(2)
Mn1−O1	2.1545(19)	Mn2−O5	2.1138(19)
Mn1−N2	2.283(2)	Mn2−N6	2.255(2)
Mn1−N1	2.259(2)	Mn2−N5	2.253(2)
Mn1−N4	2.247(2)	Mn2−N8	2.283(2)
O6−Mn1−N3	171.49(9)	O5−Mn2−N6	161.43(8)
O1−Mn1−N2	165.15(7)	O2−Mn2−N7	165.62(9)
N1−Mn1−N4	157.36 (10)	N5−Mn2−N8	161.24(10)
O6−C57−C59−C60	62.11(40)	O2−C25−C27−C32	63.28(40)
C59−C64−C58−O7	22.22(50)	C27−C28−C26−O4	33.53(40)
Mn1⋯Mn2	4.790(76)		

916

917

918

919

920   **Table 6** Selected bond lengths (Å) and angles (°) for compound 6.

921

Mn1−O1	2.172(2)	Mn1···Mn1a	6.420(1)
Mn1−O2	2.202(2)	O1−Mn1−O2	175.20(10)
Mn1−O5	2.150(3)	O6−Mn1−N1	164.38(12)
Mn1−O6	2.130(2)	O5−Mn1−N2	160.60(9)
Mn1−N1	2.275(3)	O4−C8−C6−C1	51.42(40)
Mn1−N2	2.287(4)	O1a−C7−C1−C6	57.43(40)

Symmetry codes: (a) $1 + x, y, z$.

922

923

924

925

926 **Table 7** Magnetic coupling constants and selected structural parameters for compounds with

927 the formula $[\{Mn(L)(NN)\}_2(\mu\text{-}O)(\mu\text{-}2\text{-}RC_6H_4COO)_2]X_2$.

928

R	L	NN	X	J^a (cm^{-1})	λ^b	ω^c (°)	τ^d (°)	Refs.
Cl	H_2O/H_2O	phen	ClO_4	−12.6	2.04	77.9	88.3	[28]
Cl	H_2O/ClO_4	bpy	ClO_4	−10.9	3.30	56.5	92.6	[29]
CH$_3$	H_2O/ClO_4	bpy	ClO_4	−5.6	3.45	46.9	93.6^e	[26]
COOH	H_2O/H_2O	phen	ClO_4	−3.7	2.29	22.9	91.3	this work
F	H_2O/ClO_4	bpy	ClO_4	−3.5	2.22	13.8	93.6	[26]
CH$_3$	H_2O/NO_3	bpy	NO_3	−0.5	2.10	28.8	97.2	[26]
Cl	NO_3/NO_3	phen	–	−0.3	1.36	38.1	101.7	[29]
F	H_2O/NO_3	bpy	NO_3	1.4	1.87	18.6	91.6^e	[26]
H	OH/ NO_3	bpy	NO_3	2.0	1.48	10.2	94.9	[34a]
Cl	H_2O/H_2O	phen	ClO_4	2.7	1.53	46.0	102.1	[28]
Cl	H_2O/NO_3	bpy	NO_3	3.0	1.29	25.4	108.5	[29]
COOH	H_2O/NO_3	bpy	NO_3	4.7	2.06	19.9	96.2^e	[10]
H	N_3/N_3	bpy	–	17.2	0.24	5.0	108.1	[34b]

[a] $H = -JS_1 \cdot S_2$.
[b] Distortion parameter (average values).
[c] O−C−C angle (average values).
[d] L−Mn−Mn−L angle.
[e] Average values.

929

930

931

932

933   **Table 8** Magnetic coupling constants and selected structural parameters for dinuclear Mn^{II}

934   compounds $[\{Mn(NN)_2\}_2(\mu\text{-}2\text{-}RC_6H_4COO)_2]^{2+}$.

935

R		NN	J^a (cm^{-1})	$d_{anti}{}^b$ (Å)	$d_{syn}{}^c$ (Å)	α^d (°)	β^e (°)	γ^f (°)	ω^g (°)	Refs.
H	a	bpy	−1.8	2.14	2.12	103.6	126.4	152.0	9	[31c]
Cl	b	bpy	−1.8	2.20	2.12	96.4	130.9	132.7	50	[31e]
CH$_3$	c	phen	−1.6	2.14	2.14	95.8	127.4	132.9	48	[31b]
Cl	d	phen	−1.4	2.13	2.14	94.3	123.9	131.9	57	[31b]
COOH	5	phen	−1.5	2.14	2.13	91.9	127.5	133.6	62	This work
COOH^h	e	phen	−0.3	2.12	2.13	94.7	128.3	136.9	63	[13b]

^{a} $H = -JS_1 \cdot S_2$.
^{b} $Mn-O_{anti}$ distance.
^{c} $Mn-O_{syn}$ distance.
^{d} $O_{anti}-Mn-O_{syn}$ angle.
^{e} $Mn-O_{syn}-C$ angle.
^{f} $Mn-O_{anti}-C$.
^{g} $O-C-C-C$ angle.
^{h} Phthalate as counteranion.

936

937

938

939

940 **Table 9** Magnetic coupling constants and selected structural parameters for 2D systems
941 formed by trinuclear entities.

942

Compound	Mn···Mn (Å)	Mn–O_b^a (Å)	Mn–O_d (Å)	Mn–O_b–Mn (°)	J^b (cm^{-1})	Refs.
4	3.526	2.195 2.206	2.388	106.51	−4.5	This work
Y	3.266	2.210 2.206	2.254	105.74	−^{c}	[16a]
Z	3.615	2.263 2.198	2.314	108.22	−2	[16c]

^{a} Mn$_c$–O_b and Mn$_t$–O_b distances.
^{b} $H = -J(S_1S_2 + S_2S_3)$.
^{c} Weak antiferromagnetic coupling fitted with Curie–Weiss: $C = 10.8$ cm^3 K mol^{-1}, $\theta = -1.81$ K.

943

944

945

946

Figures Captions

Figure 1. Reactivity of carboxybenzoic acids in the synthesis of Mn^{III} and Mn^{II} compounds.

Figure 2. Crystal structure of the cationic complex of compound **1**, showing the atom labelling scheme and ellipsoids at 50% probability. Carbon-bonded hydrogen atoms are omitted for clarity.

Figure 3. Hydrogen bonds present in the crystal structure of compound **1**.

Figure 4. Crystal structure of the cationic complex of compound 3, showing the atom labelling scheme and ellipsoids at 50% probability. Hydrogen atoms are omitted for clarity.

Figure 5. Two-dimensional view of compound **4** along the b axis (top) and crystal structure of a trinuclear fragment showing the atom labelling scheme and ellipsoids at 50% probability (bottom). Hydrogen atoms are omitted for clarity.

Figure 6. Crystal structure of the cationic complex of compound 5, showing the atom labelling scheme and ellipsoids at 50% probability. Carbon-bonded hydrogen atoms are omitted for clarity.

Figure 7. Crystal structure of compound 6, showing the atom labelling scheme and ellipsoids at 50% probability. Carbon-bonded hydrogen atoms are omitted for clarity.

Figure 8. $\chi_M T$ vs. T and χ_M vs. T (inset) plots for compound **1**. The solid line is the best fit to the experimental data.

Figure 9. $\chi_M T$ vs. T and χ_M vs. T (inset) plots for compounds 3 ($\circ$) and 5 ($\blacksquare$). The solid line is the best fit to the experimental data.

Scheme 1. Relative orientation of magnetic orbitals involved in the interaction through carboxylate bridges with a syn–anti conformation

Figure 10. $\chi_M T$ vs. T and χ_M vs. T (inset) plots for compound **6**. The solid line is the best fit to the experimental data.

Figure 11. $\chi_M T$ vs. T and M vs. H (inset) plots for compound **4**. The solid line is the best fit to the experimental data.

Scheme 2. Kambe's vector coupling scheme [43].

Scheme 3. Schematic structure of a trinuclear unit, the bridging and dangling metal-to-oxygen bonds being in bold.

Figure 12. X-band EPR spectra of a powdered samples of compounds **3** (top) and **5** (bottom). The dashed line is the best simulation achieved.

Figure 13. X-band EPR spectrum of a powdered sample of compound **4**. The dashed line is the best simulation achieved.

Figure 14. Evolved O_2 for compound **4** with different initial concentrations of H_2O_2: 0.50 ($\circ$), 0.60 ($\blacksquare$) and 0.70 mL ($\lozenge$).

Figure 1

$MnX_2 + NBu_4MnO_4 + NN + RC_6H_4COOH$

$[Mn(4–COOC_6H_4COO)_2]_n + HNO_3 + phen$

$MnX_2 + NN + RC_6H_4COOH$
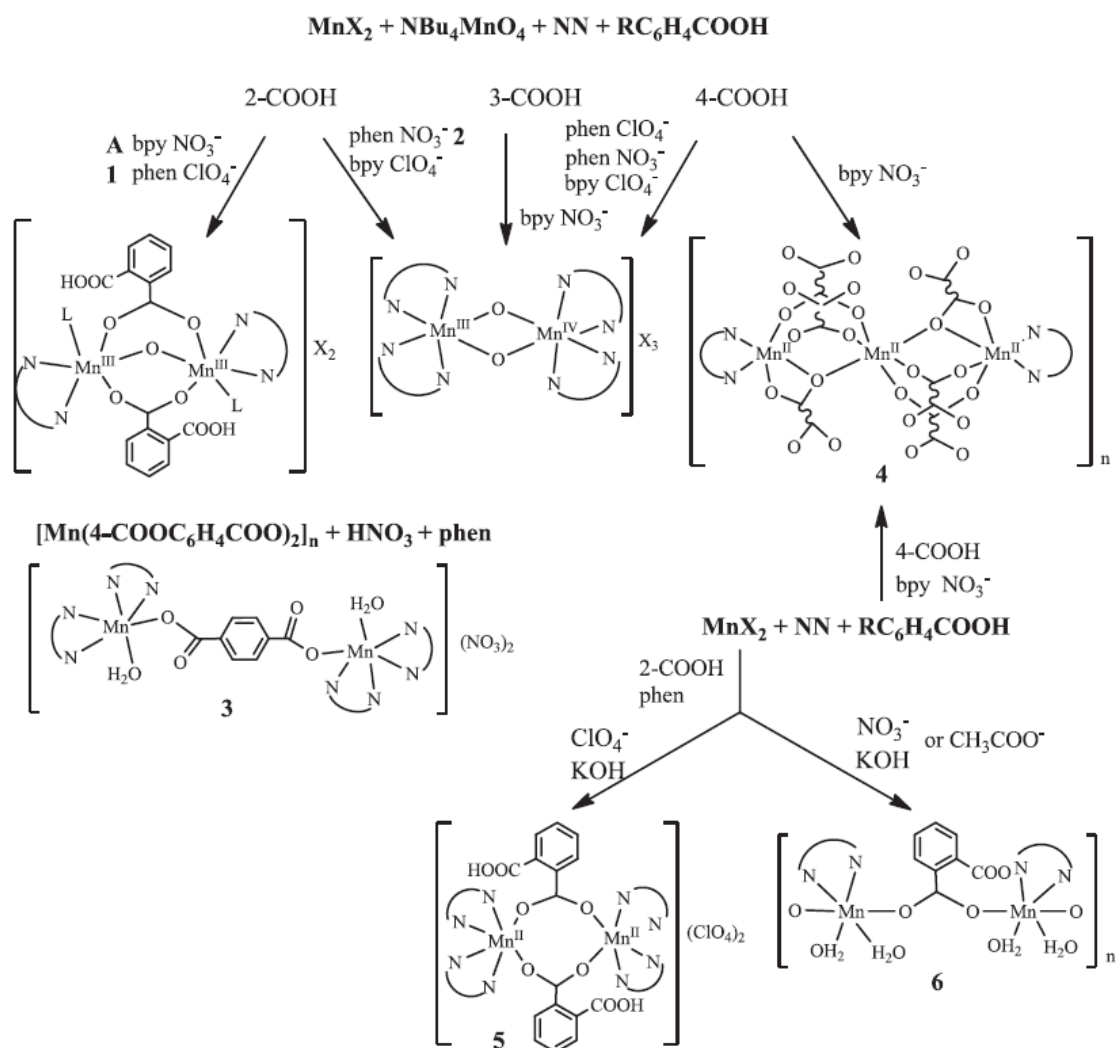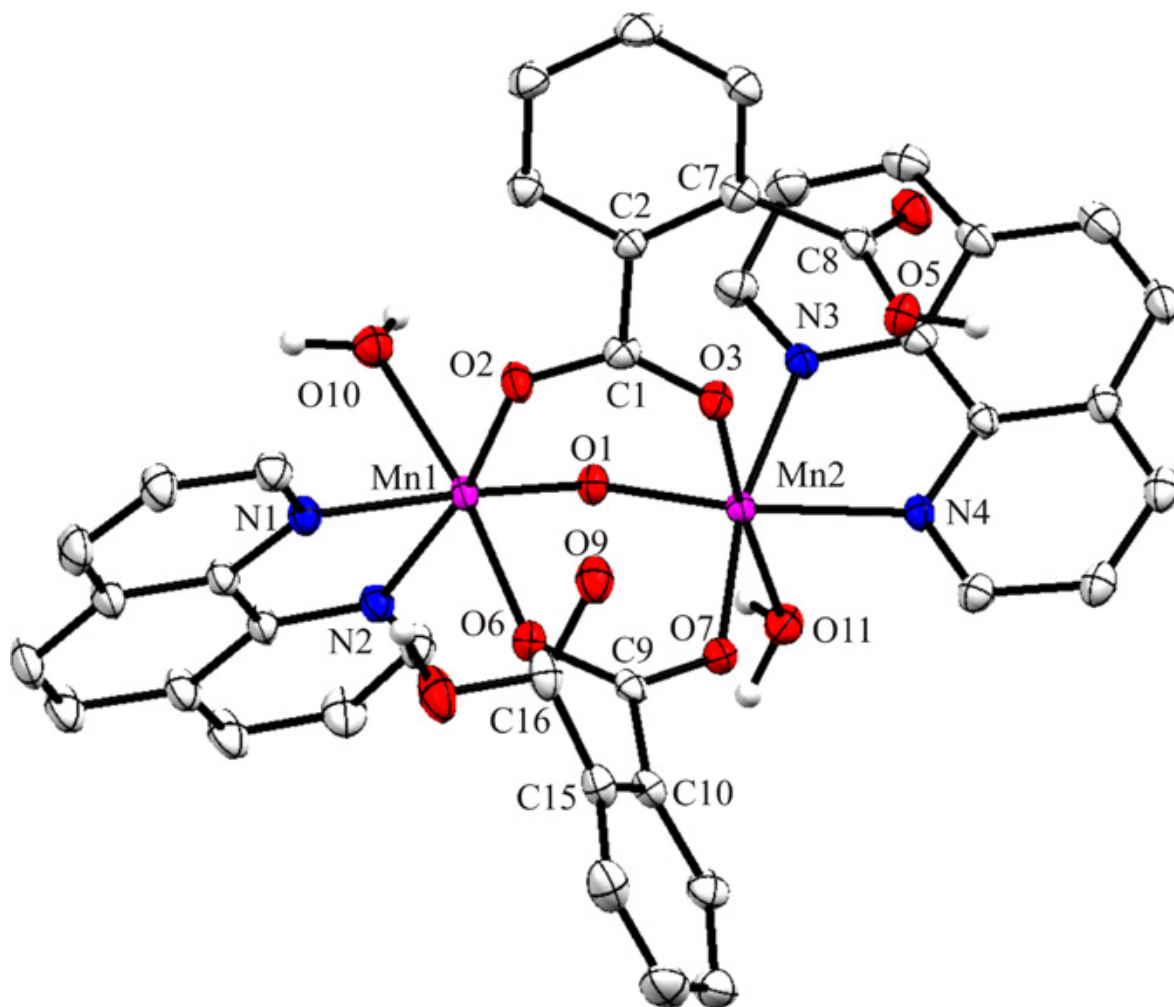
Figure 2
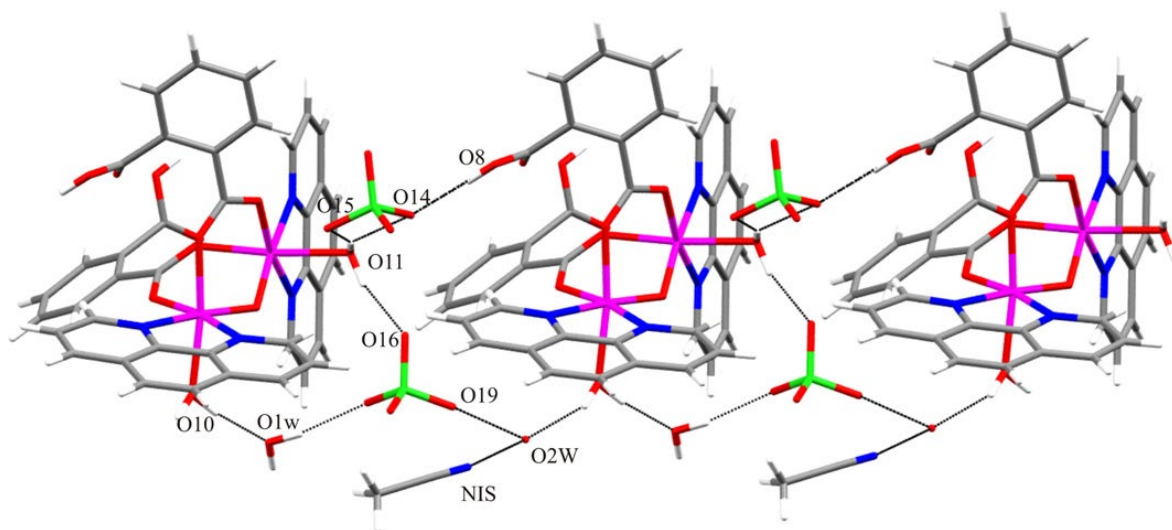
993   **Figure 3**

994

995

996

997

998

999
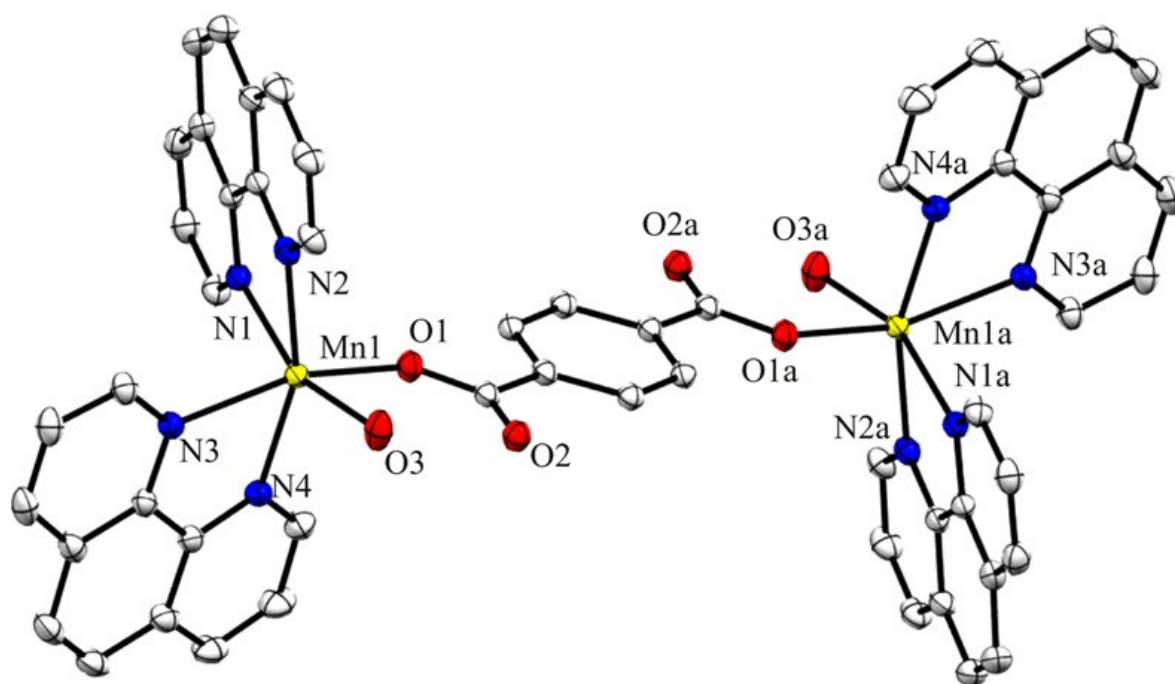
1000

1001

1002

Figure 4

Figure 5

1008
1009
1010
1011
1012
1013
1014
1015
1016
1017
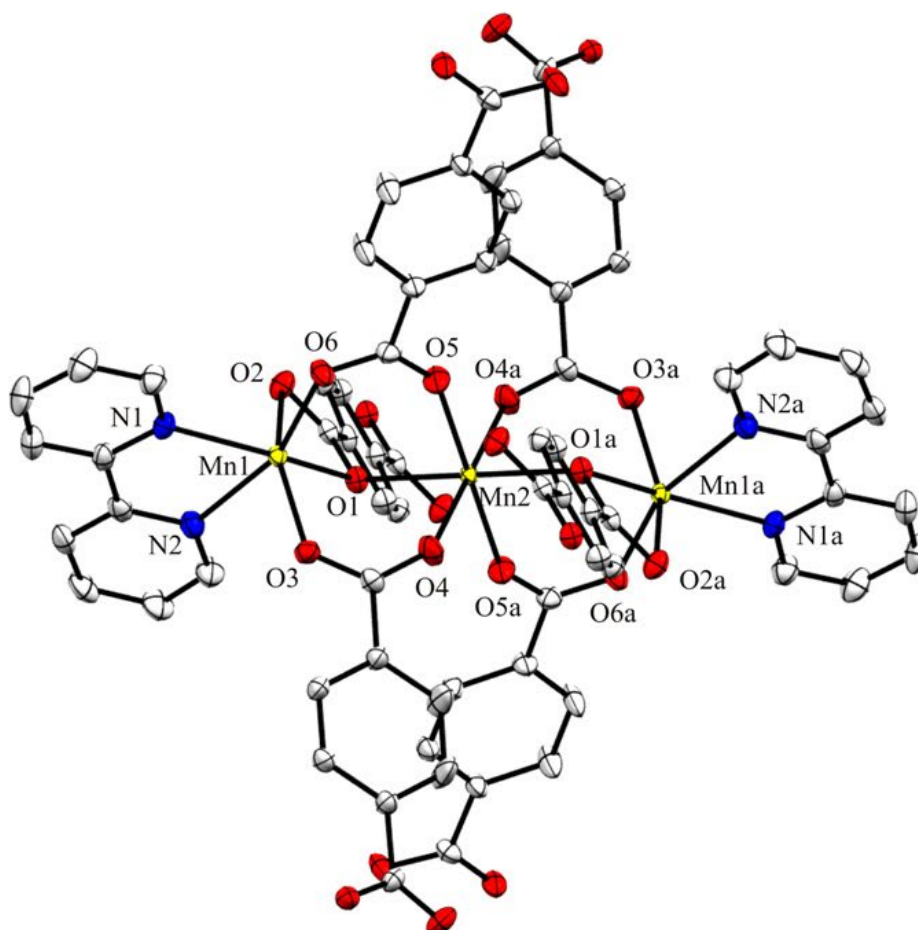1018
1019
1020
1021
1022
1023
1024
1025
1026
1027
1028
1029
1030
1031
1032
1033
1034
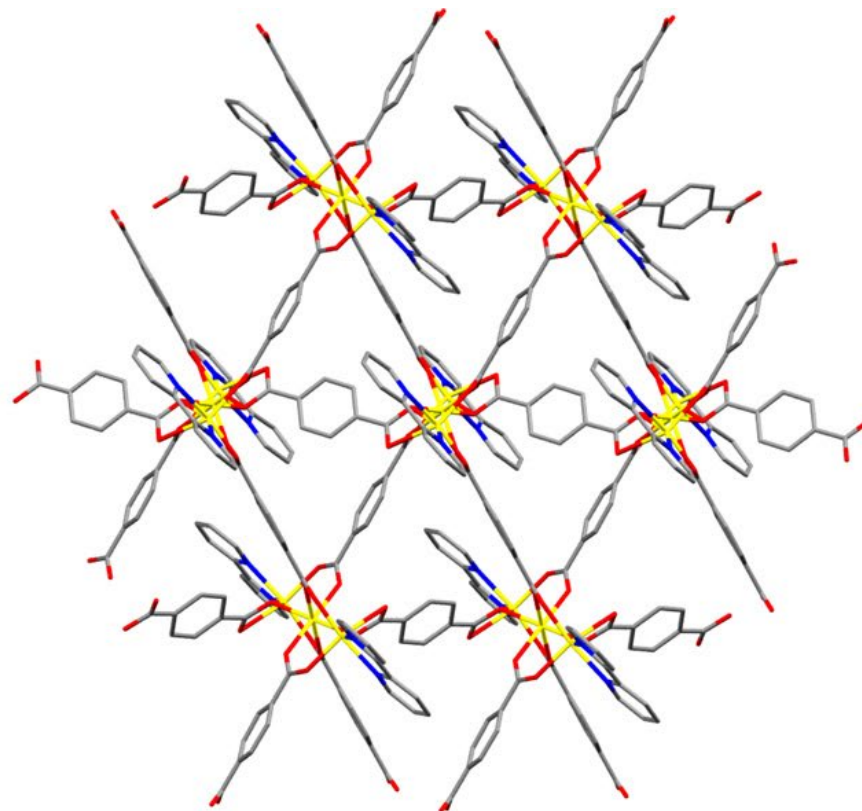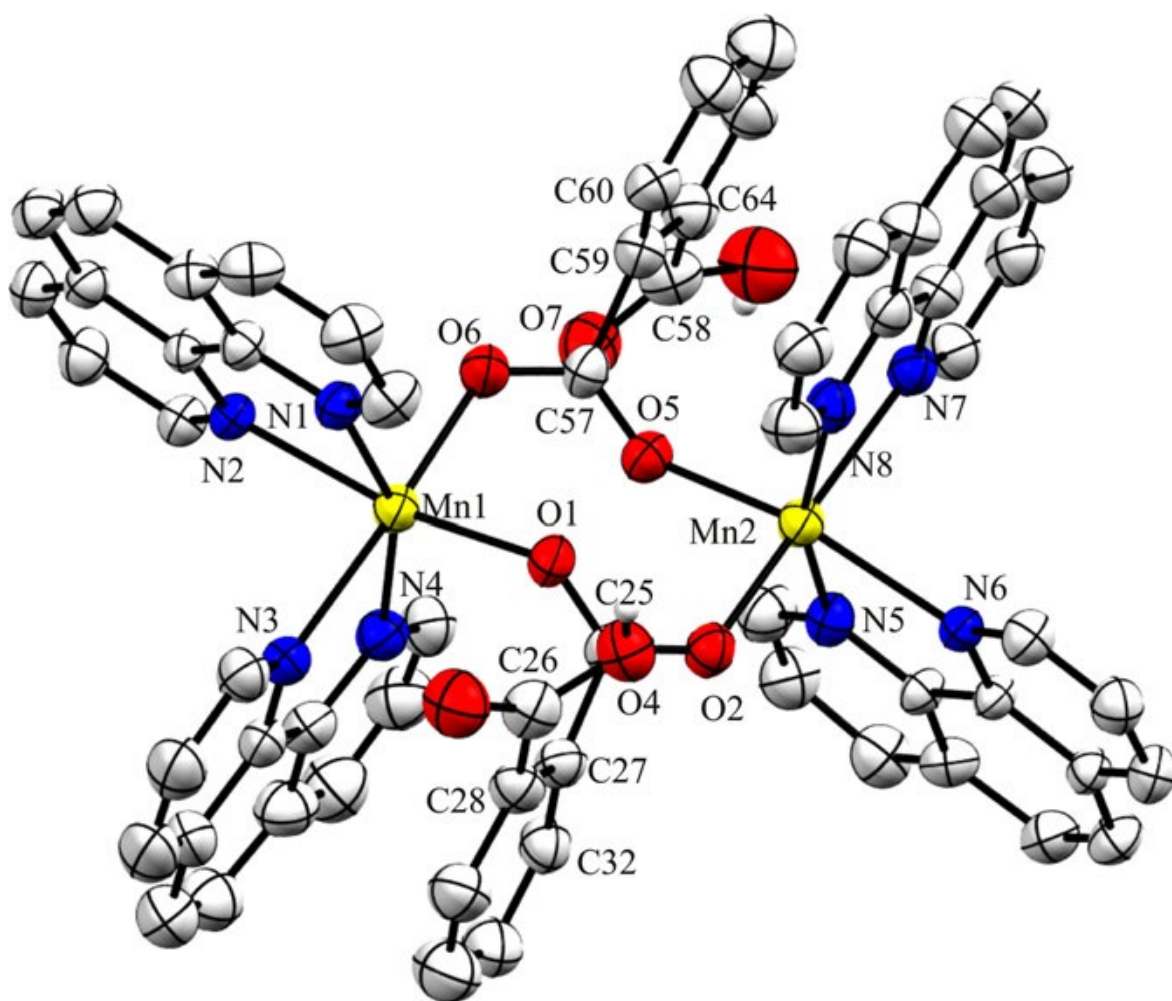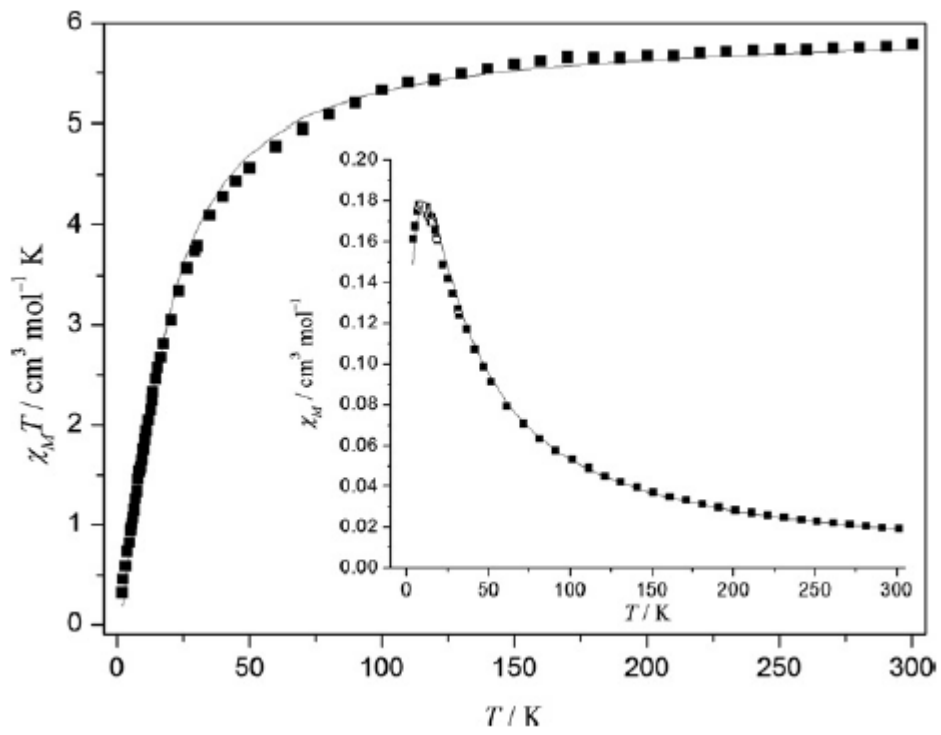1035
1036
1037

Figure 6

1039
1040
1041
1042
1043

1044   **Figure 7**

1045

1046

1047

1048

1049

1050   **Figure 8**

1051

1052

1053

1054

1055
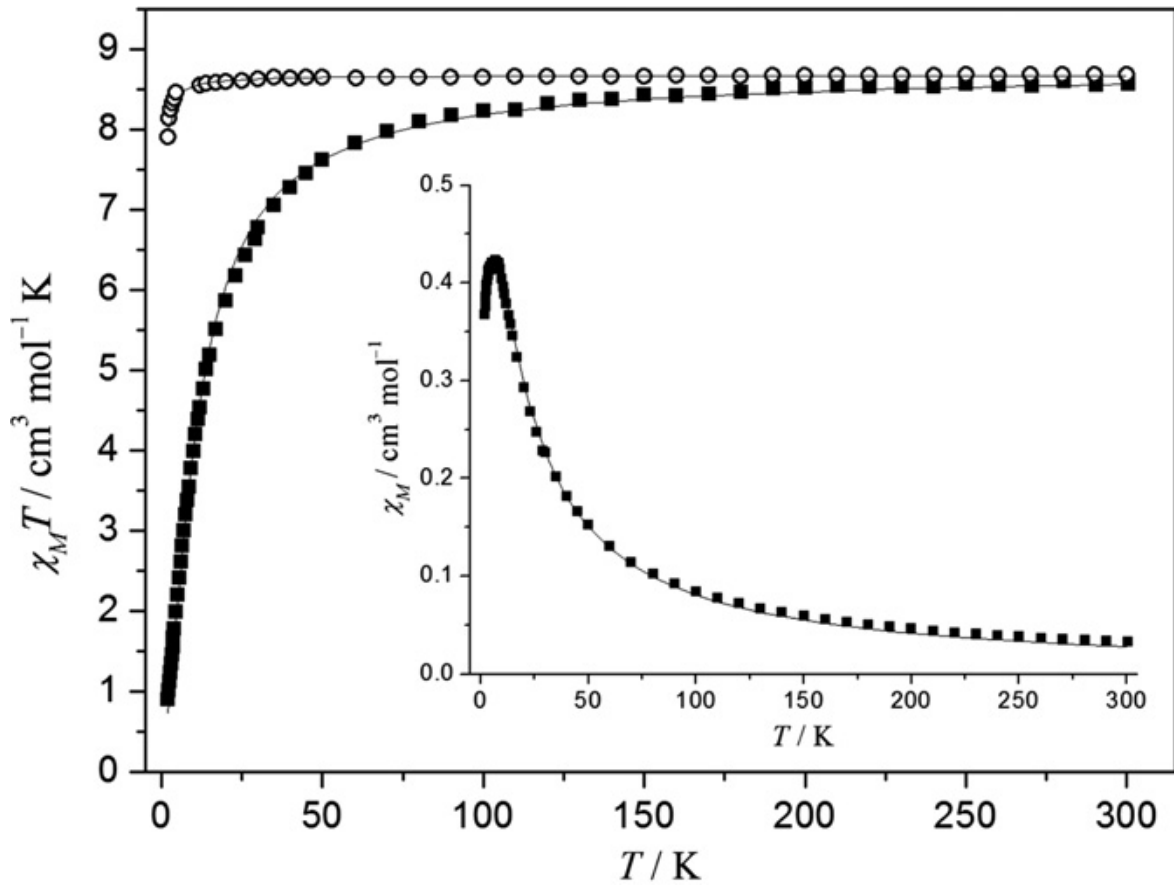
Figure 9

1062   **Scheme 1.**
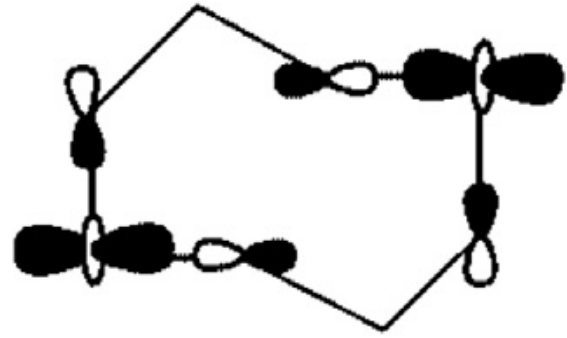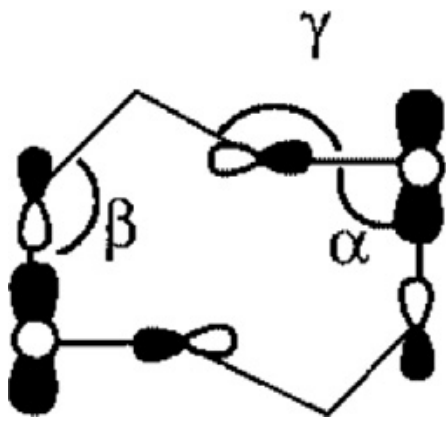
1063

1064

1065

1066   **Figure 10**
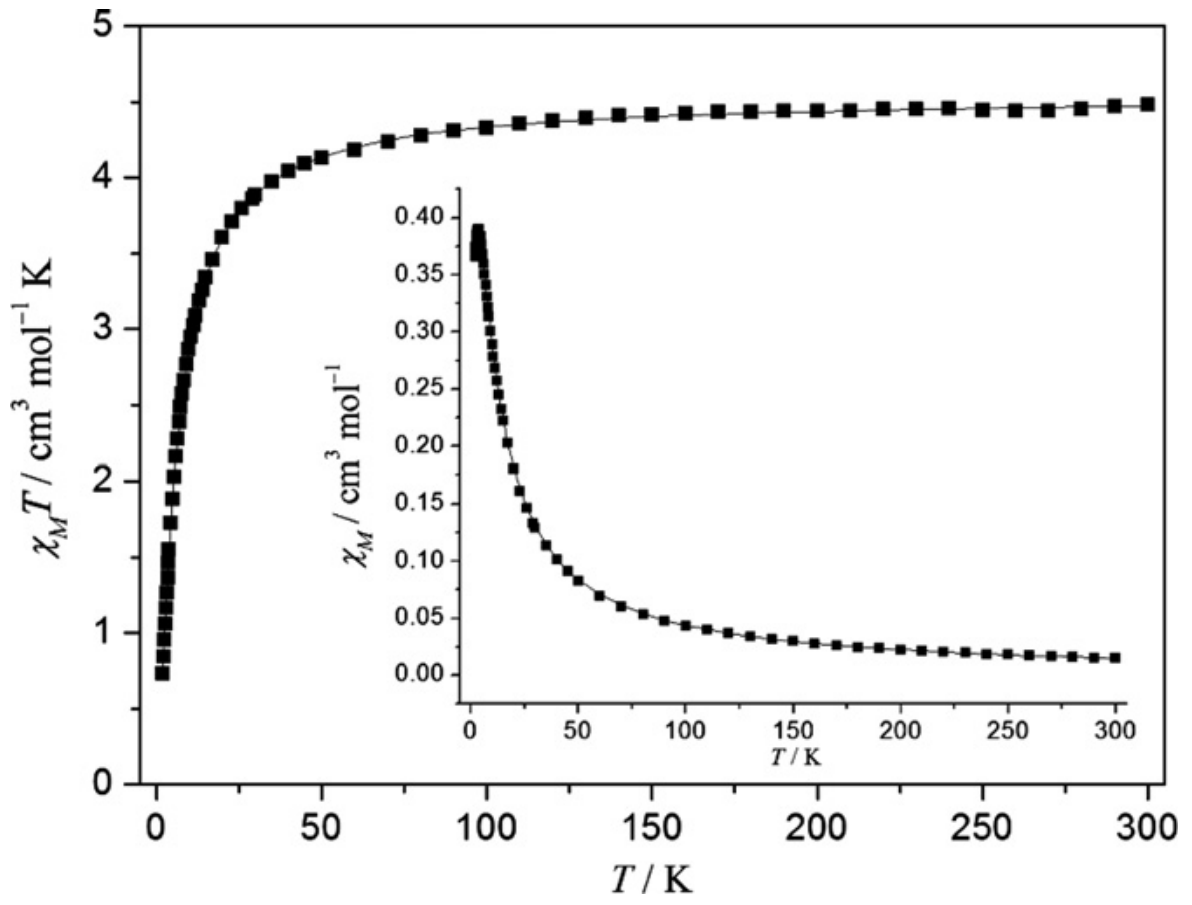
1067

1068

1069

1070

1071

Figure 11

1078   **Scheme 2.**

$$\text{Mn}_1 \xleftrightarrow{\ J\ } \text{Mn}_2 \xleftrightarrow{\ J\ } \text{Mn}_3$$

$$J_{13}$$
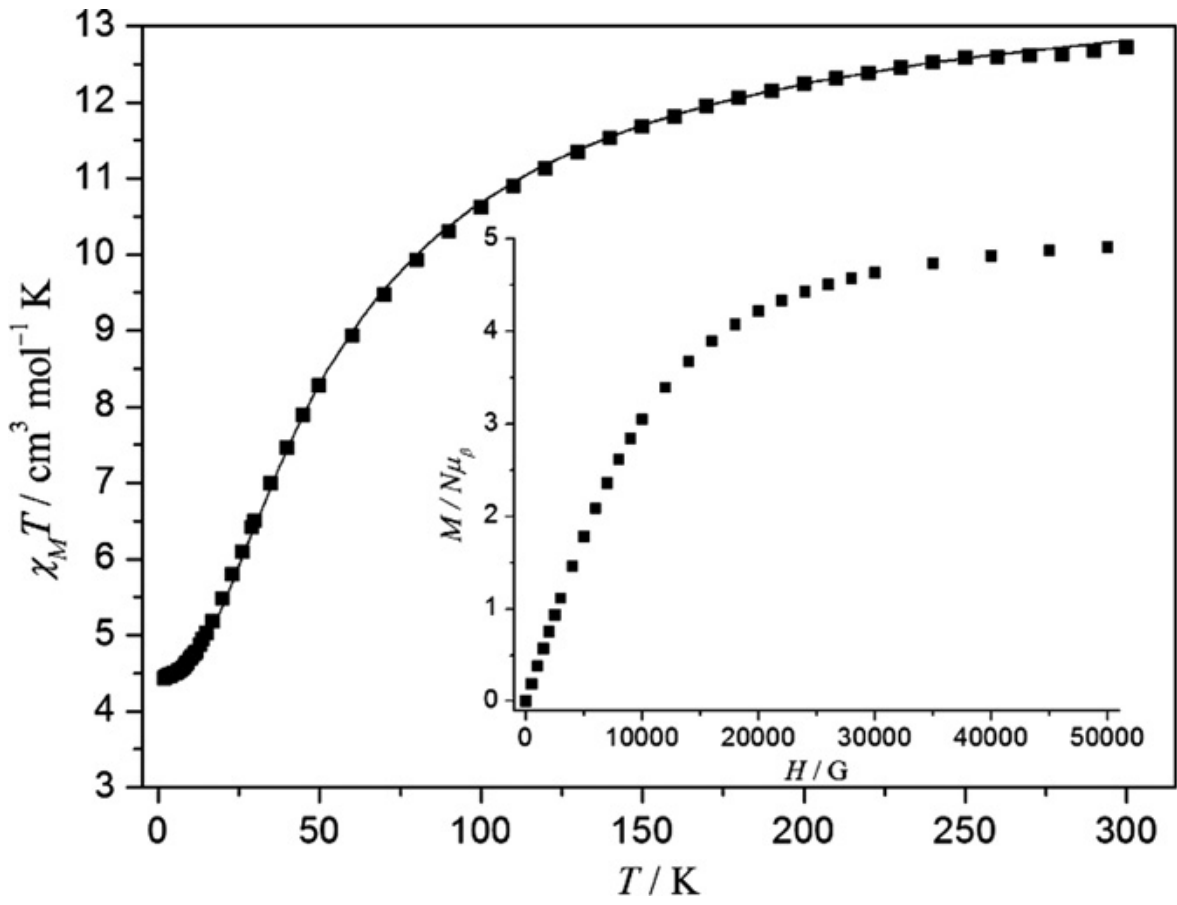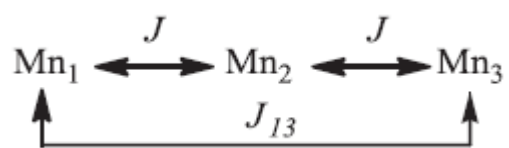
1079

1080

1081

1082   **Scheme 3.**
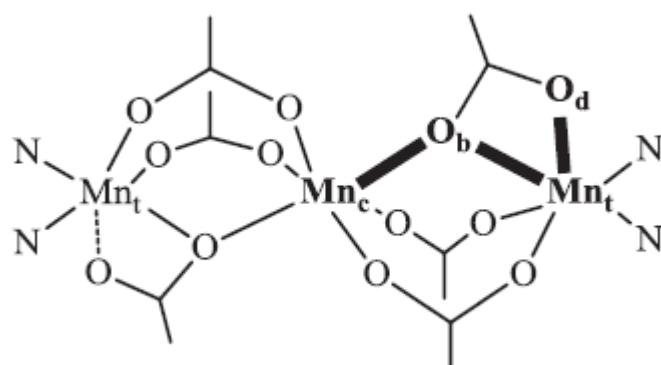
1083

1084

1085

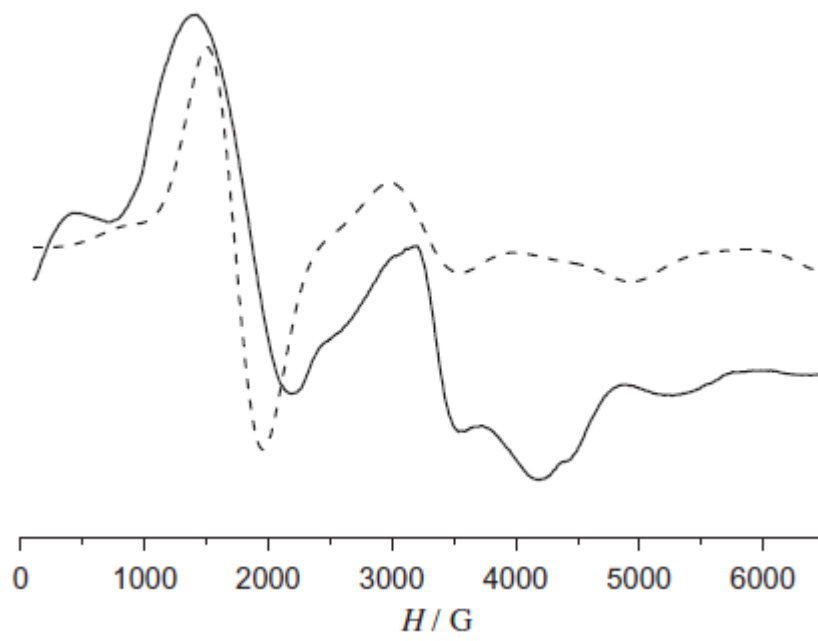1086   **Figure 12**

1087

H / G
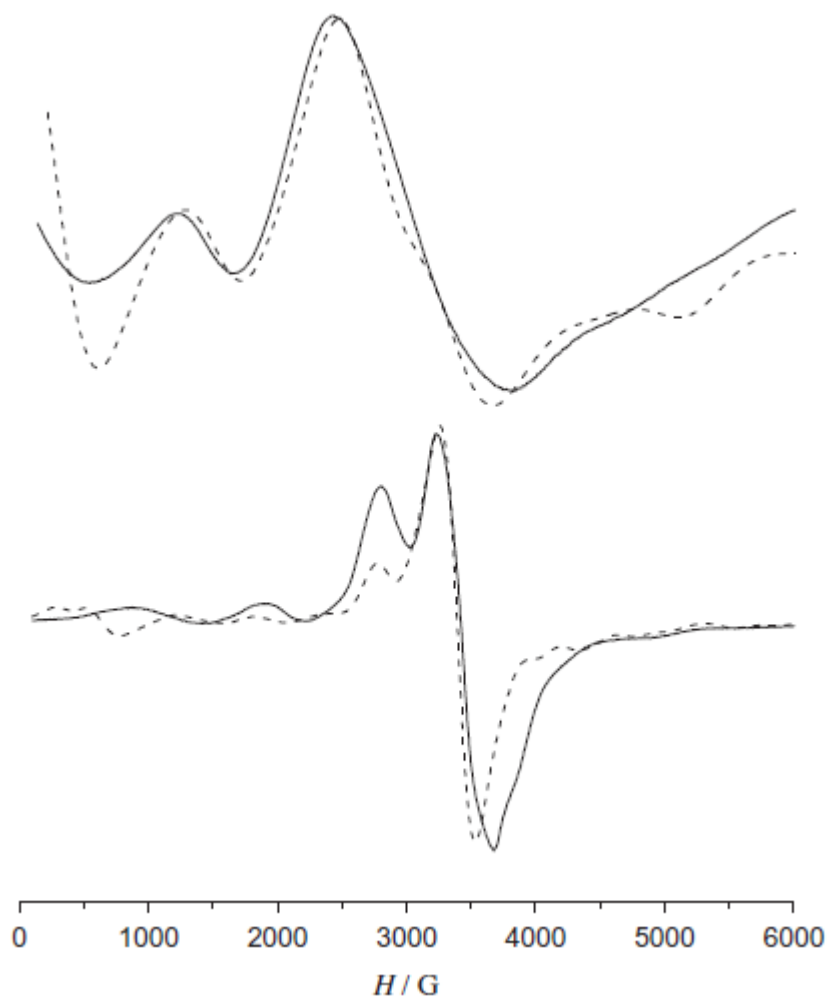
1088
1089
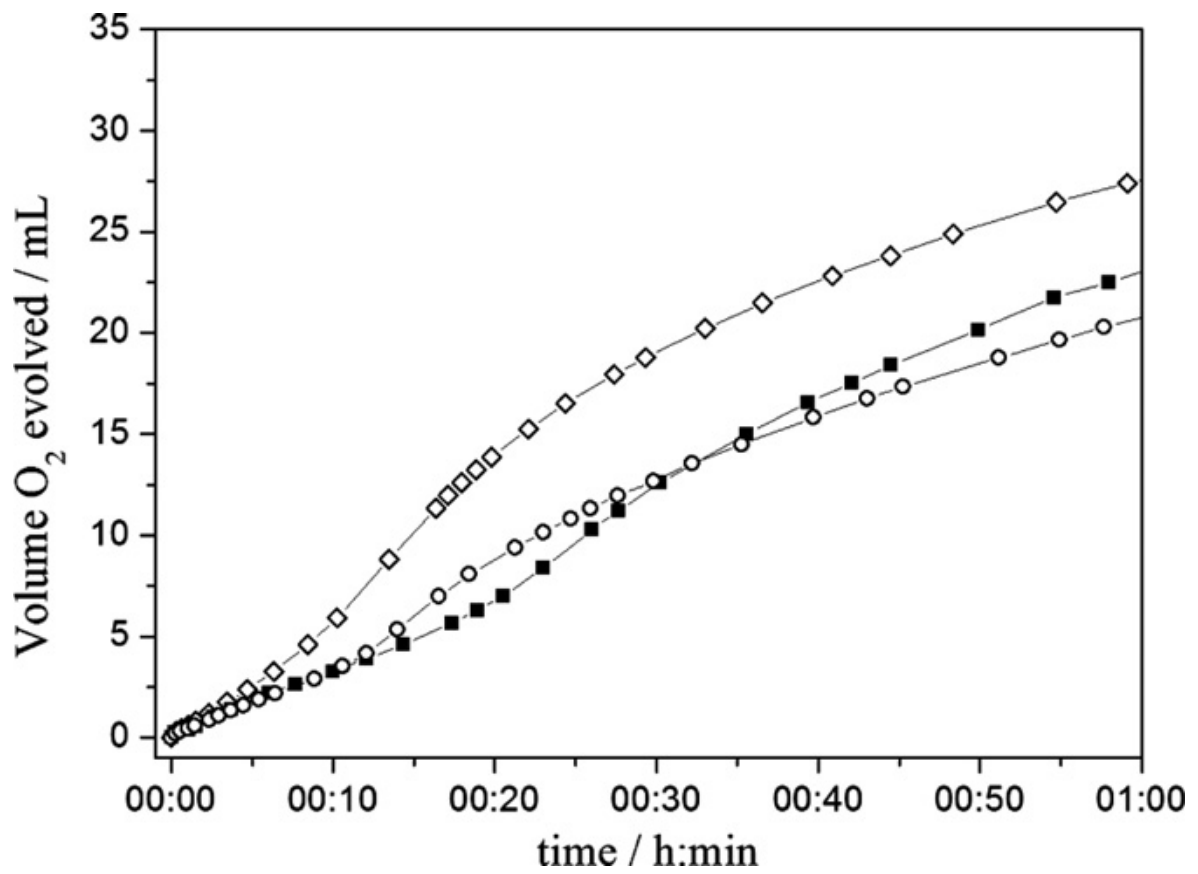1090
1091

1092   **Figure 13**

1093

1094

1095

1096

1097

1098   **Figure 14**

1099

1100

1101

1102